ASIAN JOURNAL OF CIVIL ENGINEERING (BUILDING AND HOUSING) VOL. 10, NO. 4 (2009)
PAGES 451-480

DELAMINATION IN CROSS-PLY LAMINATED BEAMS USING THE LAYERWISE THEORY

Wook Jin Na* and J.N. Reddy
Department of Mechanical Engineering, Texas A.M University, College Station, TX, USA

ABSTRACT

A finite element model based on the layerwise theory of Reddy is developed for the analysis of delamination in the $[90/0]_S$ cross-ply laminated beams. The Heaviside step function was adopted in the formulation to express the discontinuous interlaminar displacement fields of delaminated layers. Also, to accommodate the moderately large rotations of the beam, the von Kármán type nonlinear strain field is used in the formulation. The finite element model is verified by comparing the present solutions with those available in the literature. It is shown that the present finite element model is able to capture accurate local stress fields and the strain energy release rates. Then the model is used to study delaminated cross-ply laminates under bending loads. The influence of boundary conditions and number of layers on the strain energy release rates is studied. Also, the growth of delamination is investigated for a pure bending case, and the mode of delamination growth is identified. The influence of geometric nonlinearity on the delamination growth is also investigated as the delamination advances. It is found that geometric nonlinearity does not significantly alter the delamination kinematics and strain energy release rates.

Keywords: Delamination; finite element model; geometric nonlinearity; laminated composite beams; layerwise theory

1. INTRODUCTION

Free-edge delamination is observed in uniaxial tensile tests, and internal delamination is also found under various loading conditions. In many cases, interfacial cracks appear to be originated from the tips of pre-existing transverse cracks. For cross-ply laminates, 90-degree plies are susceptible to transverse cracks and they result in delamination at interfaces of the transversely cracked 90-degree plies and the adjacent 0-degree plies.

Pagano and Pipes [1] provided an analytic solution to the distribution of the interlaminar transverse normal stress along the interface of free edge delamination. They also conducted an experiment to validate the analytical solution. Kim [2, 3] reported characteristics of free edge delamination under tensile loads and attempted to give a criterion for the onset of

* E-mail address of the corresponding author: jnreddy@tamu.edu (J.N. Reddy)

delamination by a strength criterion [3]. Brewer and Lagace [4] also proposed a quadratic stress criterion for initiation of delamination.

Delamination is often analyzed in terms of the change in strain energy release rate using the principles of fracture mechanics because delamination has more similarities to crack growth in the framework of fracture mechanics than transverse matrix cracking. Unlike the matrix cracking, where the progress of damage is measured by the number of cracks in the damaged layer, the crack length is the measure of the damage growth in delamination and it is predicted by estimating the strain energy release rate.

In the frame work of fracture mechanics, Griffith [5] proposed a condition for a crack extension using the principle of minimum total potential energy $(\delta U = -\delta V)$. This condition is called Griffith criterion for a crack to grow. Griffith criterion has been mathematically and thermodynamically improved by Rice [6], who postulated a contour integral that is path independent as the change in potential energy for a virtual crack extension. This special integral is known as *J*-integral under the context of fracture mechanics. Gurtin [7] later showed that *J*-integral is equivalent to the strain energy release rate for the linear elastic material.

Applying the concept of strain energy release rate to delamination phenomenon in composite laminates, Wang [8] asserted that the rate of strain energy release during crack extension is a material property, which is known as the critical strain energy release rate. Wang and his colleagues also intensively investigated delamination phenomena related to transverse cracks and produced useful information about the strain energy release rate through a series of works [9-11]. The strain energy release rate is suggested as a criterion for delamination growth by a number of others [12-14]. Among those, Sih et al. [15] and O'Brien [16] addressed different contributions of the strain energy release rate depending on the failure mode, and pointed out that the total mixed mode strain energy release rate controls the onset of edge delamination under cyclic loads. The strain energy release rates of mixed modes are considered by Wilkins *et al*. [17] and Hahn [18].

In the present study, the characteristics of delamination in the laminated beam under bending loads are investigated for the $[90/0]_S$ cross-ply laminated beams, while accounting for von Kármán nonlinearity. The change of strain energy release rate is examined to predict the delamination growth. Also, mixture of failure modes in the laminate under bending is considered and the contribution of each mode's strain energy release rate to the total strain energy release rate is studied so that the dominant mode in delamination can be identified.

2. FORMULATION

2.1 Layerwise Theory with Heaviside Step Function

The total displacement fields of the laminated beam are assumed to be written as [19]

$$\begin{aligned} u(x,z) &= u^{LWT}(x,z) + u^{DEL}(x,z) \\ v(x,z) &= 0 \\ w(x,z) &= w^{LWT}(x,z) + w^{DEL}(x,z) \end{aligned} \tag{1}$$

where u^{LWT} and w^{LWT} are the longitudinal and the transverse displacement fields using the layerwise theory expressed as

$$u^{LWT}(x,z)=\sum_{I=1}^{N}U_I(x)\Phi^I(z) \tag{2a}$$

$$w^{LWT}(x,z)=\sum_{I=1}^{M}W_I(x)\Psi^I(z)\,. \tag{2b}$$

In equations (2a)-(2b), Φ^I and Ψ^I are generally different 1-D Lagrangian polynomials with C^0 continuity across the layers so that the strain field through the thickness can be discontinuous and the stress field can possibly continuous; u^{DEL} and w^{DEL} in equations (1a) and (1c) denote the discontinuous longitudinal and transverse displacement, respectively, due to delamination. They can be expressed as

$$u^{DEL}(x,z)=\sum_{I=1}^{ND}{}^{D}U_I(x)H(z-z_I) \tag{3a}$$

$$w^{DEL}(x,z)=\sum_{I=1}^{ND}{}^{D}W_I(x)H(z-z_I) \tag{3b}$$

where ND indicates the number of delaminated interfaces and $H(z)$ is the Heaviside step function

$$H(z-z_I)=\begin{cases}1 & , \quad z\geq z_I\\ 0 & , \quad z<z_I\end{cases}\,. \tag{4}$$

It should be noted that the Ith nodal values of (u,w) are the combination of (U_I,W_I) and $({}^{D}U_I,{}^{D}W_I)$.

To accommodate moderately large rotations of the transverse lines but with small strains, the von Kármán type nonlinear strains are employed

$$\begin{aligned}\varepsilon_{xx}=\frac{\partial u}{\partial x}+\frac{1}{2}\left(\frac{\partial w}{\partial x}\right)^2=&\sum_{I=1}^{N}\frac{dU_I(x)}{dx}\Phi^I(z)+\sum_{I=1}^{ND}\frac{d\,{}^{D}U_I(x)}{dx}H(z-z_I)\\&+\frac{1}{2}\left(\sum_{I=1}^{M}\frac{dW_I(x)}{dx}\Psi^I(z)+\sum_{I=1}^{ND}\frac{d\,{}^{D}W_I(x)}{dx}H(z-z_I)\right)\\&\times\left(\sum_{J=1}^{M}\frac{dW_J(x)}{dx}\Psi^J(z)+\sum_{J=1}^{ND}\frac{d\,{}^{D}W_J(x)}{dx}H(z-z_I)\right)\end{aligned}$$

$$\varepsilon_{zz} = \frac{\partial w}{\partial z} = \sum_{I=1}^{M} W_I(x) \frac{d\Psi^I(z)}{dz} \tag{5}$$

$$\gamma_{xz} = \frac{\partial w}{\partial x} + \frac{\partial u}{\partial z} = \sum_{I=1}^{M} \frac{dW_I(x)}{dx} \Psi^I(z) + \sum_{I=1}^{N} U_I(x) \frac{d\Phi^I(z)}{dx} + \sum_{I=1}^{ND} \frac{d^D W_I(x)}{dx} H(z - z_I)$$

$$\varepsilon_{yy} = \gamma_{xy} = \gamma_{yz} = 0$$

For the *k*th orthotropic lamina, the plane stress-reduced stress-strain relations are

$$\begin{Bmatrix} \sigma_{xx} \\ \sigma_{zz} \\ \sigma_{xz} \end{Bmatrix}^{(k)} = \begin{bmatrix} \bar{C}_{11} & \bar{C}_{13} & 0 \\ \bar{C}_{13} & \bar{C}_{33} & 0 \\ 0 & 0 & \bar{C}_{55} \end{bmatrix}^{(k)} \begin{Bmatrix} \varepsilon_{xx} \\ \varepsilon_{zz} \\ \gamma_{xz} \end{Bmatrix}^{(k)} \tag{6}$$

where $\bar{C}_{ij}^{(k)}$ are the transformed elastic coefficients.

The governing equations of the layerwise beam are derived from the principle of virtual displacements

$$0 = \delta U + \delta V \tag{7}$$

where the virtual strain energy δU and the virtual work done δV by external forces (Figure 1 shows a laminated beam under general loads) are given by

$$\delta U = \int_{x_a}^{x_b} \int_{-\frac{h}{2}}^{\frac{h}{2}} \left(\sigma_{xx} \delta \varepsilon_{xx} + \sigma_{zz} \delta \varepsilon_{zz} + \sigma_{xz} \delta \gamma_{xz} \right) dz dx \tag{8a}$$

$$\delta V = -\int_{x_a}^{x_b} \left[f_b(x) \delta u(x, -\tfrac{h}{2}) + f_t(x) \delta u(x, \tfrac{h}{2}) \right] dx$$

$$-\int_{x_a}^{x_b} \left[q_b(x) \delta w(x, -\tfrac{h}{2}) + q_t(x) \delta w(x, \tfrac{h}{2}) \right] dx \tag{8b}$$

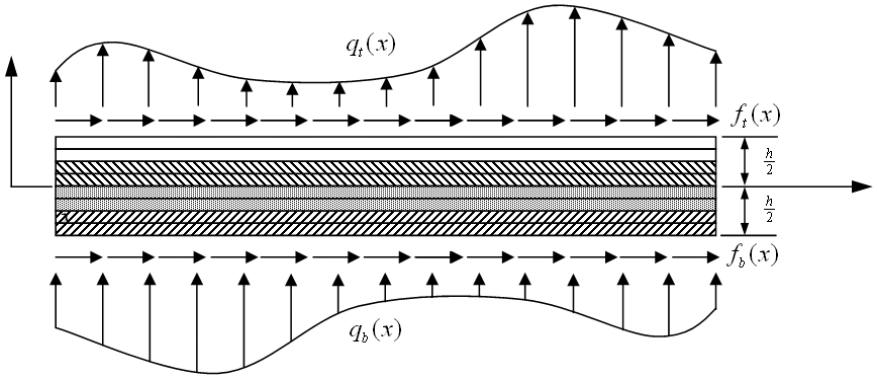

Figure 1. Laminated beam model based on the layerwise theory under general loads

Applying the stress-strain relations in equation (6) and strain-displacement relations in equations (5) to (8a) and (8b), the virtual energy and the virtual work done can be described in terms of the nodal displacements as follows:

$$\begin{aligned}\delta U = &\int_{x_a}^{x_b}\left[\sum_{I=1}^{N}\left(N_{xx}^{I}\frac{d\,\delta U_I}{dx}+Q_x^I\,\delta U_I\right)+\sum_{I=1}^{N}\left(\sum_{J=1}^{M}N_{xx}^{IJ}\frac{d\,\delta W_I}{dx}\frac{dW_J}{dx}+Q_z^I\,\delta W_I+\tilde{Q}_x^I\frac{d\,\delta W_I}{dx}\right)\right.\\ &+\int_{x_a}^{x_b}\sum_{I=1}^{M}\sum_{J=1}^{ND}{}^{D}N_{xx}^{IJ}\frac{d\,\delta W_I}{dx}\frac{d\,{}^{D}W_J}{dx}dx\\ &+\int_{x_a}^{x_b}\sum_{I=1}^{ND}\left(\sum_{J=1}^{M}{}^{D}N_{xx}^{JI}\frac{d\,\delta\,{}^{D}W_I}{dx}\frac{dW_J}{dx}+\sum_{J=1}^{ND}{}^{D}\hat{N}_{xx}^{IJ}\frac{d\,\delta\,{}^{D}W_I}{dx}\frac{d\,{}^{D}W_J}{dx}\right)dx\\ &+\int_{x_a}^{x_b}\left(\sum_{I=1}^{ND}{}^{D}N_{xx}^{I}\frac{d\,\delta\,{}^{D}U_I}{dx}+\sum_{I=1}^{ND}{}^{D}Q_x^I\frac{d\,\delta\,{}^{D}W_I}{dx}\right)dx\end{aligned} \tag{9a}$$

$$\delta V = -\int_{x_a}^{x_b}\left(f_b\,\delta U_1+f_t\,\delta U_N\right)dx-\int_{x_a}^{x_b}\left(q_b\,\delta W_1+q_t\,\delta W_M\right)dx \tag{9b}$$

where

$$\begin{aligned}N_{xx}^{I} &= \sum_{J=1}^{N}A_{11}^{IJ}\frac{dU_J}{dx}+\frac{1}{2}\sum_{J=1}^{M}\sum_{K=1}^{M}B_{11}^{IJK}\frac{dW_J}{dx}\frac{dW_K}{dx}+\sum_{J=1}^{M}\tilde{A}_{13}^{IJ}W_J+\sum_{J=1}^{ND}{}^{D}A_{11}^{IJ}\frac{d\,{}^{D}U_J}{dx}\\ &\quad+\sum_{J=1}^{M}\sum_{K=1}^{ND}{}^{D}B_{11}^{IJK}\frac{dW_J}{dx}\frac{d\,{}^{D}W_K}{dx}+\frac{1}{2}\sum_{J=1}^{ND}\sum_{K=1}^{ND}{}^{D}\bar{B}_{11}^{IJK}\frac{d\,{}^{D}W_J}{dx}\frac{d\,{}^{D}W_K}{dx}\\ N_{xx}^{IJ} &= \sum_{K=1}^{N}B_{11}^{KIJ}\frac{dU_K}{dx}+\frac{1}{2}\sum_{K=1}^{M}\sum_{L=1}^{M}D_{11}^{IJKL}\frac{dW_K}{dx}\frac{dW_L}{dx}+\sum_{K=1}^{M}\tilde{B}_{13}^{IJK}W_K+\sum_{K=1}^{ND}{}^{D}\hat{B}_{11}^{IJK}\frac{d\,{}^{D}U_K}{dx}\\ &\quad+\sum_{K=1}^{M}\sum_{L=1}^{ND}{}^{D}D_{11}^{IJKL}\frac{dW_K}{dx}\frac{d\,{}^{D}W_L}{dx}+\frac{1}{2}\sum_{K=1}^{ND}\sum_{L=1}^{ND}{}^{D}\bar{D}_{11}^{IJKL}\frac{d\,{}^{D}W_K}{dx}\frac{d\,{}^{D}W_L}{dx}\\ {}^{D}N_{xx}^{I} &= \sum_{J=1}^{N}{}^{D}A_{11}^{JI}\frac{dU_J}{dx}+\frac{1}{2}\sum_{J=1}^{M}\sum_{K=1}^{M}{}^{D}\hat{B}_{11}^{JKI}\frac{dW_J}{dx}\frac{dW_K}{dx}+\sum_{J=1}^{M}{}^{D}\tilde{A}_{13}^{IJ}W_J+\sum_{J=1}^{ND}{}^{D}\bar{A}_{11}^{IJ}\frac{d\,{}^{D}U_J}{dx}\\ &\quad+\sum_{J=1}^{M}\sum_{K=1}^{ND}{}^{D}\hat{\bar{B}}_{11}^{JIK}\frac{dW_J}{dx}\frac{d\,{}^{D}W_K}{dx}+\frac{1}{2}\sum_{J=1}^{ND}\sum_{K=1}^{ND}{}^{D}\bar{\bar{B}}_{11}^{IJK}\frac{d\,{}^{D}W_J}{dx}\frac{d\,{}^{D}W_K}{dx}\\ {}^{D}N_{xx}^{IJ} &= \sum_{K=1}^{N}{}^{D}B_{11}^{KIJ}\frac{dU_K}{dx}+\frac{1}{2}\sum_{K=1}^{M}\sum_{L=1}^{M}{}^{D}D_{11}^{IKLJ}\frac{dW_K}{dx}\frac{dW_L}{dx}+\sum_{K=1}^{M}{}^{D}\tilde{B}_{13}^{IJK}W_K+\sum_{K=1}^{ND}{}^{D}\hat{\bar{B}}_{11}^{IJK}\frac{d\,{}^{D}U_K}{dx}\\ &\quad+\sum_{K=1}^{M}\sum_{L=1}^{ND}{}^{D}\bar{D}_{11}^{IKJL}\frac{dW_K}{dx}\frac{d\,{}^{D}W_L}{dx}+\frac{1}{2}\sum_{K=1}^{ND}\sum_{L=1}^{ND}{}^{D}\bar{\bar{D}}_{11}^{IJKL}\frac{d\,{}^{D}W_K}{dx}\frac{d\,{}^{D}W_L}{dx}\\ {}^{D}\hat{N}_{xx}^{IJ} &= \sum_{K=1}^{N}{}^{D}\bar{B}_{11}^{KIJ}\frac{dU_K}{dx}+\frac{1}{2}\sum_{K=1}^{M}\sum_{L=1}^{M}{}^{D}\bar{D}_{11}^{KLIJ}\frac{dW_K}{dx}\frac{dW_L}{dx}+\sum_{K=1}^{M}{}^{D}\tilde{\bar{B}}_{13}^{IJK}W_K+\sum_{K=1}^{ND}{}^{D}\bar{\bar{B}}_{11}^{IJK}\frac{d\,{}^{D}U_K}{dx}\end{aligned}$$

$$+\sum_{K=1}^{M}\sum_{L=1}^{ND} {}^{D}\bar{\bar{D}}_{11}^{KIJL}\frac{dW_K}{dx}\frac{d\,{}^{D}W_L}{dx}+\frac{1}{2}\sum_{K=1}^{ND}\sum_{L=1}^{ND} {}^{D}\bar{\bar{\bar{D}}}_{11}^{IJKL}\frac{d\,{}^{D}W_K}{dx}\frac{d\,{}^{D}W_L}{dx}$$

$$Q_x^I=\sum_{J=1}^{N}\bar{A}_{55}^{IJ}U_J+\sum_{J=1}^{M}\bar{B}_{55}^{IJ}\frac{dW_J}{dx}+\sum_{J=1}^{ND} {}^{D}\bar{B}_{55}^{IJ}\frac{d\,{}^{D}W_J}{dx}$$

$$\tilde{Q}_x^I=\sum_{J=1}^{N}\bar{B}_{55}^{JI}U_J+\sum_{J=1}^{M}\bar{D}_{55}^{IJ}\frac{dW_J}{dx}+\sum_{J=1}^{ND} {}^{D}\bar{A}_{55}^{IJ}\frac{d\,{}^{D}W_J}{dx}$$

$$Q_z^I=\sum_{J=1}^{N}\tilde{A}_{31}^{JI}\frac{dU_J}{dx}+\frac{1}{2}\sum_{J=1}^{M}\sum_{K=1}^{M}\tilde{B}_{31}^{JKI}\frac{dW_J}{dx}\frac{dW_K}{dx}+\sum_{J=1}^{M}\hat{A}_{33}^{IJ}W_J+\sum_{J=1}^{ND} {}^{D}\tilde{A}_{31}^{JI}\frac{d\,{}^{D}U_J}{dx}$$

$$+\sum_{J=1}^{M}\sum_{K=1}^{ND} {}^{D}\tilde{B}_{31}^{JKI}\frac{dW_J}{dx}\frac{d\,{}^{D}W_K}{dx}+\frac{1}{2}\sum_{J=1}^{ND}\sum_{K=1}^{ND} {}^{D}\tilde{\bar{B}}_{31}^{JKI}\frac{d\,{}^{D}W_J}{dx}\frac{d\,{}^{D}W_K}{dx}$$

$${}^{D}Q_x^I=\sum_{J=1}^{N} {}^{D}\bar{B}_{55}^{JI}U_J+\sum_{J=1}^{M} {}^{D}\bar{A}_{55}^{JI}\frac{dW_J}{dx}+\sum_{J=1}^{ND} {}^{D}\bar{\bar{A}}_{55}^{IJ}\frac{d\,{}^{D}W_J}{dx} \tag{10}$$

and

$$A_{ij}^{IJ}=\sum_{k=1}^{Ne}\int_{z_k}^{z_{k+1}}\bar{C}_{ij}^{(k)}\Phi^I\Phi^J dz$$

$$\tilde{A}_{ij}^{IJ}=\sum_{k=1}^{Ne}\int_{z_k}^{z_{k+1}}\bar{C}_{ij}^{(k)}\Phi^I\frac{d\Psi^J}{dz}dz$$

$$\bar{A}_{ij}^{IJ}=\sum_{k=1}^{Ne}\int_{z_k}^{z_{k+1}}\bar{C}_{ij}^{(k)}\frac{d\Phi^I}{dz}\frac{d\Phi^J}{dz}dz$$

$$\hat{A}_{ij}^{IJ}=\sum_{k=1}^{Ne}\int_{z_k}^{z_{k+1}}\bar{C}_{ij}^{(k)}\frac{d\Psi^I}{dz}\frac{d\Psi^J}{dz}dz$$

$$\bar{B}_{ij}^{IJ}=\sum_{k=1}^{Ne}\int_{z_k}^{z_{k+1}}\bar{C}_{ij}^{(k)}\frac{d\Phi^I}{dz}\Psi^J dz$$

$$\bar{D}_{ij}^{IJ}=\sum_{k=1}^{Ne}\int_{z_k}^{z_{k+1}}\bar{C}_{ij}^{(k)}\Psi^I\Psi^J dz$$

$$B_{ij}^{IJK}=\sum_{k=1}^{Ne}\int_{z_k}^{z_{k+1}}\bar{C}_{ij}^{(k)}\Phi^I\Psi^J\Psi^K dz$$

$$\tilde{B}_{ij}^{IJK}=\sum_{k=1}^{Ne}\int_{z_k}^{z_{k+1}}\bar{C}_{ij}^{(k)}\Psi^I\Psi^J\frac{d\Psi^K}{dz}dz$$

$$D_{ij}^{IJKL}=\sum_{k=1}^{Ne}\int_{z_k}^{z_{k+1}}\bar{C}_{ij}^{(k)}\Psi^I\Psi^J\Psi^K\Psi^L dz$$

$${}^{D}A_{ij}^{IJ}=\sum_{k=1}^{Ne}\int_{z_k}^{z_{k+1}}\bar{C}_{ij}^{(k)}\Phi^I H^J dz$$

$${}^{D}\bar{A}_{ij}^{IJ}=\sum_{k=1}^{Ne}\int_{z_k}^{z_{k+1}}\bar{C}_{ij}^{(k)}\Psi^I H^J dz$$

$$
\begin{aligned}
{}^{D}\tilde{A}_{ij}^{IJ} &= \sum_{k=1}^{Ne}\int_{z_k}^{z_{k+1}} \bar{C}_{ij}^{(k)} H^{I}\,\frac{d\Psi^{J}}{dz}\,dz \\
{}^{D}\bar{\bar{A}}_{ij}^{IJ} &= \sum_{k=1}^{Ne}\int_{z_k}^{z_{k+1}} \bar{C}_{ij}^{(k)} H^{I} H^{J}\,dz \\
{}^{D}\bar{B}_{ij}^{IJ} &= \sum_{k=1}^{Ne}\int_{z_k}^{z_{k+1}} \bar{C}_{ij}^{(k)}\,\frac{d\Phi^{I}}{dz} H^{J}\,dz \\
{}^{D}B_{ij}^{IJK} &= \sum_{k=1}^{Ne}\int_{z_k}^{z_{k+1}} \bar{C}_{ij}^{(k)} \Phi^{I}\Psi^{J} H^{K}\,dz \\
{}^{D}\bar{B}_{ij}^{IJK} &= \sum_{k=1}^{Ne}\int_{z_k}^{z_{k+1}} \bar{C}_{ij}^{(k)} \Phi^{I} H^{J} H^{K}\,dz \\
{}^{D}\bar{\bar{B}}_{ij}^{IJK} &= \sum_{k=1}^{Ne}\int_{z_k}^{z_{k+1}} \bar{C}_{ij}^{(k)} H^{I} H^{J} H^{K}\,dz \\
{}^{D}\hat{B}_{ij}^{IJK} &= \sum_{k=1}^{Ne}\int_{z_k}^{z_{k+1}} \bar{C}_{ij}^{(k)} \Psi^{I}\Psi^{J} H^{K}\,dz \\
{}^{D}\hat{\hat{B}}_{ij}^{IJK} &= \sum_{k=1}^{Ne}\int_{z_k}^{z_{k+1}} \bar{C}_{ij}^{(k)} \Psi^{I} H^{J} H^{K}\,dz \\
{}^{D}\tilde{B}_{ij}^{IJK} &= \sum_{k=1}^{Ne}\int_{z_k}^{z_{k+1}} \bar{C}_{ij}^{(k)} \Psi^{I} H^{J}\,\frac{d\Psi^{K}}{dz}\,dz \\
{}^{D}\tilde{\tilde{B}}_{ij}^{IJK} &= \sum_{k=1}^{Ne}\int_{z_k}^{z_{k+1}} \bar{C}_{ij}^{(k)} H^{I} H^{J}\,\frac{d\Psi^{K}}{dz}\,dz \\
{}^{D}D_{ij}^{IJKL} &= \sum_{k=1}^{Ne}\int_{z_k}^{z_{k+1}} \bar{C}_{ij}^{(k)} \Psi^{I}\Psi^{J}\Psi^{K} H^{L}\,dz \\
{}^{D}\bar{D}_{ij}^{IJKL} &= \sum_{k=1}^{Ne}\int_{z_k}^{z_{k+1}} \bar{C}_{ij}^{(k)} \Psi^{I}\Psi^{J} H^{K} H^{L}\,dz \\
{}^{D}\bar{\bar{D}}_{ij}^{IJKL} &= \sum_{k=1}^{Ne}\int_{z_k}^{z_{k+1}} \bar{C}_{ij}^{(k)} \Psi^{I} H^{J} H^{K} H^{L}\,dz \\
{}^{D}\bar{\bar{\bar{D}}}_{ij}^{IJKL} &= \sum_{k=1}^{Ne}\int_{z_k}^{z_{k+1}} \bar{C}_{ij}^{(k)} H^{I} H^{J} H^{K} H^{L}\,dz\,. \qquad (11)
\end{aligned}
$$

where, Ne is the number of physical layers in the laminate. The laminate stiffness coefficients with three or four superscripts are introduced to include nonlinear strains. The superscript D in front of the laminate stiffness coefficients indicates that the terms correspond to delamination.

2.2 Finite Element Model

In the finite element method, the beam is divided into a number of finite elements, and over each beam element the displacements are approximated by expansions of the form

$$U_I(x)=\sum_{j=1}^{p}U_I^j\varphi_j^{(1)}(x),\qquad W_I(x)=\sum_{j=1}^{q}W_I^j\varphi_j^{(2)}(x) \tag{12a}$$

$$^{D}U_I(x)=\sum_{j=1}^{r}{}^{D}U_I^j\varphi_j^{(3)}(x),\quad {}^{D}W_I(x)=\sum_{j=1}^{s}{}^{D}W_I^j\varphi_j^{(4)}(x) \tag{12b}$$

where p and q are the number of nodes per 1-D element used to approximate the longitudinal and transverse deflections, respectively, and r and s are the number of nodes per 1-D element used to approximate the discontinuous longitudinal and transverse deflections due to delamination, respectively; U_I^j, W_I^j, ${}^{D}U_I^j$ and ${}^{D}W_I^j$ are the amplitudes of displacements at the jth node along the longitudinal (x) direction of the Ith beam element. The interpolation functions $\varphi_j^{(m)}(m=1,2,3,4)$ denote the 1-D Lagrangian polynomials associated with jth node of the element.

Substituting the approximated displacement fields (12a)-(12d) in the longitudinal direction and their variational forms into δU and δV of equations (9a) and (9b) yields the finite element equations for a typical element as

$$\begin{bmatrix}[K^{(11)}] & [K^{(12)}] & [K^{(13)}] & [K^{(14)}]\\ [K^{(21)}] & [K^{(22)}] & [K^{(23)}] & [K^{(24)}]\\ [K^{(31)}] & [K^{(32)}] & [K^{(33)}] & [K^{(34)}]\\ [K^{(41)}] & [K^{(42)}] & [K^{(43)}] & [K^{(44)}]\end{bmatrix}^{e}\begin{Bmatrix}\{U\}\\ \{W\}\\ \{{}^{D}U\}\\ \{{}^{D}W\}\end{Bmatrix}^{e}=\begin{Bmatrix}\{{}^{1}F\}\\ \{{}^{2}F\}\\ \{0\}\\ \{0\}\end{Bmatrix}^{e} \tag{13}$$

where

$$K_{ij}^{(11)IJ}=\int_{x_a}^{x_b}\left(A_{11}^{IJ}\frac{d\varphi_i^{(1)}}{dx}\frac{d\varphi_j^{(1)}}{dx}+\bar{A}_{55}^{IJ}\varphi_i^{(1)}\varphi_j^{(1)}\right)dx$$

$$K_{ij}^{(12)IJ}=\int_{x_a}^{x_b}\left[\frac{1}{2}\left(\sum_{K=1}^{M}B_{11}^{IJK}\frac{dW_K}{dx}\right)\frac{d\varphi_i^{(1)}}{dx}\frac{d\varphi_j^{(2)}}{dx}+\tilde{A}_{13}^{IJ}\frac{d\varphi_i^{(1)}}{dx}\varphi_j^{(2)}+\bar{B}_{55}^{IJ}\varphi_i^{(1)}\frac{d\varphi_j^{(2)}}{dx}\right]dx$$

$$+\int_{x_a}^{x_b}\left(\sum_{K=1}^{ND}{}^{D}B_{11}^{IJK}\frac{d\,{}^{D}W_K}{dx}\right)\frac{d\varphi_i^{(1)}}{dx}\frac{d\varphi_j^{(2)}}{dx}dx$$

$$K_{ij}^{(13)IJ}=\int_{x_a}^{x_b}{}^{D}A_{11}^{IJ}\frac{d\varphi_i^{(1)}}{dx}\frac{d\varphi_j^{(3)}}{dx}dx$$

$$K_{ij}^{(14)IJ}=\int_{x_a}^{x_b}\left[\frac{1}{2}\left(\sum_{K=1}^{ND}{}^{D}B_{11}^{IJK}\frac{d\,{}^{D}W_K}{dx}\right)\frac{d\varphi_i^{(1)}}{dx}\frac{d\varphi_j^{(4)}}{dx}+{}^{D}\bar{B}_{55}^{IJ}\varphi_i^{(1)}\frac{d\varphi_j^{(4)}}{dx}\right]dx$$

$$K_{ij}^{(21)IJ}=\int_{x_a}^{x_b}\left[\left(\sum_{K=1}^{M}B_{11}^{JIK}\frac{dW_K}{dx}\right)\frac{d\varphi_i^{(2)}}{dx}\frac{d\varphi_j^{(1)}}{dx}+\tilde{A}_{31}^{JI}\varphi_i^{(2)}\frac{d\varphi_j^{(1)}}{dx}+\bar{B}_{55}^{JI}\frac{d\varphi_i^{(2)}}{dx}\varphi_j^{(1)}\right]dx$$
$$+\int_{x_a}^{x_b}\left(\sum_{K=1}^{ND}{}^{D}B_{11}^{JIK}\frac{d\,{}^{D}W_K}{dx}\right)\frac{d\varphi_i^{(2)}}{dx}\frac{d\varphi_j^{(1)}}{dx}dx$$

$$K_{ij}^{(22)IJ}=\int_{x_a}^{x_b}\left[\frac{1}{2}\left(\sum_{K=1}^{M}\sum_{L=1}^{M}D_{11}^{IJKL}\frac{dW_K}{dx}\frac{dW_L}{dx}\right)\frac{d\varphi_i^{(2)}}{dx}\frac{d\varphi_j^{(2)}}{dx}\right]dx$$
$$+\int_{x_a}^{x_b}\left[\left(\sum_{K=1}^{M}\tilde{B}_{13}^{IKJ}\frac{dW_K}{dx}\right)\frac{d\varphi_i^{(2)}}{dx}\varphi_j^{(2)}dx+\frac{1}{2}\left(\sum_{K=1}^{M}\tilde{B}_{31}^{JKI}\frac{dW_K}{dx}\right)\varphi_i^{(2)}\frac{d\varphi_j^{(2)}}{dx}\right]dx$$
$$+\int_{x_a}^{x_b}\left[\hat{A}_{33}^{IJ}\varphi_i^{(2)}\varphi_j^{(2)}+\bar{D}_{55}^{IJ}\frac{d\varphi_i^{(2)}}{dx}\frac{d\varphi_j^{(2)}}{dx}\right]dx$$
$$+\int_{x_a}^{x_b}\left[\frac{3}{2}\left(\sum_{K=1}^{M}\sum_{L=1}^{ND}{}^{D}D_{11}^{IJKL}\frac{dW_K}{dx}\frac{d\,{}^{D}W_L}{dx}\right)\frac{d\varphi_i^{(2)}}{dx}\frac{d\varphi_j^{(2)}}{dx}\right]dx$$
$$+\int_{x_a}^{x_b}\left[\left(\sum_{K=1}^{ND}{}^{D}\tilde{B}_{13}^{JKI}\frac{d\,{}^{D}W_K}{dx}\right)\varphi_i^{(2)}\frac{d\varphi_j^{(2)}}{dx}+\left(\sum_{K=1}^{ND}{}^{D}\tilde{B}_{13}^{IKJ}\frac{d\,{}^{D}W_K}{dx}\right)\frac{d\varphi_i^{(2)}}{dx}\varphi_j^{(2)}\right]dx$$
$$+\int_{x_a}^{x_b}\left[\left(\sum_{K=1}^{ND}\sum_{L=1}^{ND}{}^{D}\bar{D}_{11}^{IJKL}\frac{d\,{}^{D}W_K}{dx}\frac{d\,{}^{D}W_L}{dx}\right)\frac{d\varphi_i^{(2)}}{dx}\frac{d\varphi_j^{(2)}}{dx}\right]dx$$

$$K_{ij}^{(23)IJ}=\int_{x_a}^{x_b}\left[\left(\sum_{K=1}^{M}{}^{D}\hat{B}_{11}^{IKJ}\frac{dW_K}{dx}\right)\frac{d\varphi_i^{(2)}}{dx}\frac{d\varphi_j^{(3)}}{dx}+{}^{D}\tilde{A}_{31}^{JI}\varphi_i^{(2)}\frac{d\varphi_j^{(3)}}{dx}\right]dx$$
$$+\left(\sum_{K=1}^{ND}{}^{D}\hat{\tilde{B}}_{55}^{IKJ}\frac{d\,{}^{D}W_K}{dx}\right)\frac{d\varphi_i^{(2)}}{dx}\frac{d\varphi_j^{(3)}}{dx}\Bigg]dx$$

$$K_{ij}^{(24)IJ}=\int_{x_a}^{x_b}\left[\frac{1}{2}\left(\sum_{K=1}^{M}\sum_{L=1}^{ND}{}^{D}\bar{D}_{11}^{IKJL}\frac{dW_K}{dx}\frac{d\,{}^{D}W_L}{dx}\right)\frac{d\varphi_i^{(2)}}{dx}\frac{d\varphi_j^{(4)}}{dx}\right]dx$$
$$+\int_{x_a}^{x_b}\left[\frac{1}{2}\left(\sum_{K=1}^{ND}{}^{D}\tilde{\tilde{B}}_{31}^{JKI}\frac{d\,{}^{D}W_K}{dx}\right)\varphi_i^{(2)}\frac{d\varphi_j^{(4)}}{dx}+{}^{D}\bar{A}_{55}^{IJ}\frac{d\varphi_i^{(2)}}{dx}\frac{d\varphi_j^{(4)}}{dx}\right]dx$$
$$+\int_{x_a}^{x_b}\left[\frac{1}{2}\left(\sum_{K=1}^{ND}\sum_{L=1}^{ND}{}^{D}\bar{\bar{D}}_{11}^{IJKL}\frac{d\,{}^{D}W_K}{dx}\frac{d\,{}^{D}W_L}{dx}\right)\frac{d\varphi_i^{(2)}}{dx}\frac{d\varphi_j^{(4)}}{dx}\right]dx$$

$$K_{ij}^{(31)IJ}=\int_{x_a}^{x_b}{}^{D}A_{11}^{JI}\frac{d\varphi_i^{(3)}}{dx}\frac{d\varphi_j^{(1)}}{dx}dx$$

$$K_{ij}^{(32)IJ}=\int_{x_a}^{x_b}\left[\frac{1}{2}\left(\sum_{K=1}^{M}{}^{D}\hat{B}_{11}^{JKI}\frac{dW_K}{dx}\right)\frac{d\varphi_i^{(3)}}{dx}\frac{d\varphi_j^{(2)}}{dx}+{}^{D}\tilde{A}_{13}^{IJ}\frac{d\varphi_i^{(3)}}{dx}\varphi_j^{(2)}\right]dx$$

$$+\int_{x_a}^{x_b}\left(\sum_{K=1}^{ND} {}^{D}\hat{\hat{B}}_{11}^{JKI}\frac{d\,{}^{D}W_K}{dx}\right)\frac{d\varphi_i^{(3)}}{dx}\frac{d\varphi_j^{(2)}}{dx}dx$$

$$K_{ij}^{(33)IJ}=\int_{x_a}^{x_b} {}^{D}\bar{\bar{A}}_{11}^{IJ}\frac{d\varphi_i^{(3)}}{dx}\frac{d\varphi_j^{(3)}}{dx}dx$$

$$K_{ij}^{(34)IJ}=\int_{x_a}^{x_b}\frac{1}{2}\left(\sum_{K=1}^{ND} {}^{D}\bar{\bar{B}}_{11}^{IJK}\frac{d\,{}^{D}W_K}{dx}\right)\frac{d\varphi_i^{(3)}}{dx}\frac{d\varphi_j^{(4)}}{dx}dx$$

$$K_{ij}^{(41)IJ}=\int_{x_a}^{x_b}\left[\left(\sum_{K=1}^{ND} {}^{D}B_{11}^{JIK}\frac{d\,{}^{D}W_K}{dx}\right)\frac{d\varphi_i^{(4)}}{dx}\frac{d\varphi_j^{(1)}}{dx}+{}^{D}\bar{B}_{55}^{JI}\frac{d\varphi_i^{(4)}}{dx}\varphi_j^{(1)}\right]dx$$

$$K_{ij}^{(42)IJ}=\int_{x_a}^{x_b}\left[\frac{1}{2}\left(\sum_{K=1}^{M}\sum_{L=1}^{M} {}^{D}D_{11}^{JKLI}\frac{dW_K}{dx}\frac{dW_L}{dx}\right)\frac{d\varphi_i^{(4)}}{dx}\frac{d\varphi_j^{(2)}}{dx}\right]dx$$

$$+\int_{x_a}^{x_b}\left[\left(\sum_{K=1}^{M} {}^{D}\tilde{B}_{13}^{JIK}W_K\right)\frac{d\varphi_i^{(4)}}{dx}\frac{d\varphi_j^{(2)}}{dx}+\left(\sum_{K=1}^{ND} {}^{D}\tilde{\tilde{B}}_{13}^{IKJ}\frac{d\,{}^{D}W_K}{dx}\right)\frac{d\varphi_i^{(4)}}{dx}\varphi_j^{(2)}\right]dx$$

$$+\int_{x_a}^{x_b}\left[\left(\sum_{K=1}^{ND}\sum_{L=1}^{ND} {}^{D}\bar{\bar{D}}_{11}^{JIKL}\frac{d\,{}^{D}W_K}{dx}\frac{d\,{}^{D}W_L}{dx}\right)\frac{d\varphi_i^{(4)}}{dx}\frac{d\varphi_j^{(2)}}{dx}+{}^{D}\bar{A}_{55}^{JI}\frac{d\varphi_i^{(4)}}{dx}\frac{d\varphi_j^{(2)}}{dx}\right]dx$$

$$+\int_{x_a}^{x_b}\left[\left(\sum_{K=1}^{N} {}^{D}B_{11}^{KJI}\frac{dU_K}{dx}\right)\frac{d\varphi_i^{(4)}}{dx}\frac{d\varphi_j^{(2)}}{dx}+\left(\sum_{K=1}^{ND} {}^{D}\hat{\hat{B}}_{11}^{JIK}\frac{d\,{}^{D}U_K}{dx}\right)\frac{d\varphi_i^{(4)}}{dx}\frac{d\varphi_j^{(2)}}{dx}\right]dx$$

$$+\int_{x_a}^{x_b}\frac{1}{2}\left(\sum_{K=1}^{M}\sum_{L=1}^{ND} {}^{D}\bar{D}_{11}^{KJIL}\frac{dW_K}{dx}\frac{d\,{}^{D}W_L}{dx}\right)\frac{d\varphi_i^{(4)}}{dx}\frac{d\varphi_j^{(2)}}{dx}dx$$

$$K_{ij}^{(43)IJ}=\int_{x_a}^{x_b}\left(\sum_{K=1}^{ND} {}^{D}\bar{\bar{B}}_{11}^{IJK}\frac{d\,{}^{D}W_K}{dx}\right)\frac{d\varphi_i^{(4)}}{dx}\frac{d\varphi_j^{(3)}}{dx}dx$$

$$K_{ij}^{(44)IJ}=\int_{x_a}^{x_b}\left[\left(\sum_{K=1}^{M}\sum_{L=1}^{M} {}^{D}\bar{D}_{11}^{LKIJ}\frac{dW_K}{dx}\frac{dW_L}{dx}\right)\frac{d\varphi_i^{(4)}}{dx}\frac{d\varphi_j^{(4)}}{dx}+{}^{D}\bar{\bar{A}}_{55}^{IJ}\frac{d\varphi_i^{(4)}}{dx}\frac{d\varphi_j^{(4)}}{dx}\right.$$

$$+\frac{1}{2}\left(\sum_{K=1}^{M}\sum_{L=1}^{ND} {}^{D}\bar{\bar{D}}_{11}^{KIJL}\frac{dW_K}{dx}\frac{d\,{}^{D}W_L}{dx}\right)\frac{d\varphi_i^{(4)}}{dx}\frac{d\varphi_j^{(4)}}{dx}$$

$$\left.+\frac{1}{2}\left(\sum_{K=1}^{ND}\sum_{L=1}^{ND} {}^{D}\bar{\bar{D}}_{11}^{IJKL}\frac{d\,{}^{D}W_K}{dx}\frac{d\,{}^{D}W_L}{dx}\right)\frac{d\varphi_i^{(4)}}{dx}\frac{d\varphi_j^{(4)}}{dx}\right]dx \tag{14}$$

and

$$ {}^{1}F_i^I = \begin{cases} \int_{x_a}^{x_b} f_b(x)\varphi_i^{(1)}dx & (I=1) \\ \int_{x_a}^{x_b} f_t(x)\varphi_i^{(1)}dx & (I=N) \\ 0 & (I=2,3,\cdots,N-1) \end{cases} \tag{15a} $$

$$ {}^{2}F_i^I = \begin{cases} \int_{x_a}^{x_b} q_b(x)\varphi_i^{(2)}dx & (I=1) \\ \int_{x_a}^{x_b} q_t(x)\varphi_i^{(2)}dx & (I=M) \\ 0 & (I=2,3,\cdots,M-1) \end{cases} \tag{15b} $$

Note that the coefficient matrices contain nonlinearity in such a way that they are functions of the unknowns $U(x)$, $W(x)$, ${}^{D}U(x)$, ${}^{D}W(x)$ and their derivatives with respect to the coordinate *x*.

Equations (13)–(15) are used to compute the nonlinear response of laminated beams. The nonlinear finite element equations are solved using Newton-Raphson iterative method [20]. The tangent matrix coefficients for the nonlinear layerwise beam model are

$$ T_{ij}^{(11)IJ} = K_{ij}^{(11)IJ} $$

$$ T_{ij}^{(12)IJ} = \int_{x_a}^{x_b} \frac{1}{2}\left(\sum_{K=1}^{M} B_{11}^{IKJ}\frac{dW_K}{dx}\right)\frac{d\varphi_i^{(1)}}{dx}\frac{d\varphi_j^{(2)}}{dx}dx + K_{ij}^{(12)IJ} $$

$$ T_{ij}^{(13)IJ} = K_{ij}^{(13)IJ} $$

$$ T_{ij}^{(14)IJ} = \int_{x_a}^{x_b}\left[\left(\sum_{K=1}^{M} {}^{D}B_{11}^{IKJ}\frac{dW_K}{dx}\right)\frac{d\varphi_i^{(1)}}{dx}\frac{d\varphi_j^{(4)}}{dx} + \frac{1}{2}\left(\sum_{K=1}^{ND} {}^{D}\bar{B}_{11}^{IJK}\frac{d\,{}^{D}W_K}{dx}\right)\frac{d\varphi_i^{(1)}}{dx}\frac{d\varphi_j^{(4)}}{dx}\right]dx + K_{ij}^{(14)IJ} $$

$$ T_{ij}^{(21)IJ} = K_{ij}^{(21)IJ} $$

$$ \begin{aligned} T_{ij}^{(22)IJ} = \int_{x_a}^{x_b}\Bigg[&\left(\sum_{K=1}^{N} B_{11}^{KIJ}\frac{dU_K}{dx}\right)\frac{d\varphi_i^{(2)}}{dx}\frac{d\varphi_j^{(2)}}{dx} + \left(\sum_{K=1}^{M}\sum_{L=1}^{M} D_{11}^{IKJL}\frac{dW_K}{dx}\frac{dW_L}{dx}\right)\frac{d\varphi_i^{(2)}}{dx}\frac{d\varphi_j^{(2)}}{dx} \\ &+\left(\sum_{K=1}^{M}\tilde{B}_{13}^{IJK}W_K\right)\frac{d\varphi_i^{(2)}}{dx}\frac{d\varphi_j^{(2)}}{dx} + \frac{1}{2}\left(\sum_{K=1}^{M}\tilde{B}_{31}^{KJI}\frac{dW_K}{dx}\right)\varphi_i^{(2)}\frac{d\varphi_j^{(2)}}{dx} \\ &+\frac{3}{2}\left(\sum_{K=1}^{M}\sum_{L=1}^{ND} {}^{D}D_{11}^{IKJL}\frac{dW_K}{dx}\frac{d\,{}^{D}W_L}{dx}\right)\frac{d\varphi_i^{(2)}}{dx}\frac{d\varphi_j^{(2)}}{dx} + \left(\sum_{K=1}^{ND} {}^{D}\hat{B}_{13}^{IJK}\frac{d\,{}^{D}U_K}{dx}\right)\frac{d\varphi_i^{(2)}}{dx}\frac{d\varphi_j^{(2)}}{dx} \end{aligned} $$

$$+\frac{1}{2}\left(\sum_{K=1}^{ND}\sum_{L=1}^{ND} {}^{D}\bar{D}_{11}^{IJKL}\frac{d\,{}^{D}W_K}{dx}\frac{d\,{}^{D}W_L}{dx}\right)\frac{d\varphi_i^{(2)}}{dx}\frac{d\varphi_j^{(2)}}{dx}\Bigg]dx + K_{ij}^{(22)IJ}$$

$$T_{ij}^{(23)IJ} = K_{ij}^{(23)IJ}$$

$$T_{ij}^{(24)IJ} = \int_{x_a}^{x_b}\Bigg[\left(\sum_{K=1}^{N} {}^{D}B_{11}^{KIJ}\frac{dU_K}{dx}\right)\frac{d\varphi_i^{(2)}}{dx}\frac{d\varphi_j^{(4)}}{dx}+\frac{3}{2}\left(\sum_{K=1}^{M}\sum_{L=1}^{M} {}^{D}D_{11}^{ILKJ}\frac{dW_K}{dx}\frac{dW_L}{dx}\right)\frac{d\varphi_i^{(2)}}{dx}\frac{d\varphi_j^{(4)}}{dx}$$
$$+\left(\sum_{K=1}^{M} {}^{D}\tilde{B}_{31}^{KJI}\frac{dW_K}{dx}\right)\varphi_i^{(2)}\frac{d\varphi_j^{(4)}}{dx}+\left(\sum_{K=1}^{M} {}^{D}\tilde{B}_{13}^{IJK}W_K\right)\frac{d\varphi_i^{(2)}}{dx}\frac{d\varphi_j^{(4)}}{dx}$$
$$+2\left(\sum_{K=1}^{M}\sum_{L=1}^{ND} {}^{D}\bar{D}_{11}^{IKJL}\frac{dW_K}{dx}\frac{d\,{}^{D}W_L}{dx}\right)\frac{d\varphi_i^{(2)}}{dx}\frac{d\varphi_j^{(4)}}{dx}+\left(\sum_{K=1}^{ND} {}^{D}\hat{\hat{B}}_{11}^{IJK}\frac{d\,{}^{D}U_K}{dx}\right)\frac{d\varphi_i^{(2)}}{dx}\frac{d\varphi_j^{(4)}}{dx}$$
$$+\frac{1}{2}\left(\sum_{K=1}^{M}\sum_{L=1}^{ND} {}^{D}\bar{D}_{11}^{IKLJ}\frac{dW_K}{dx}\frac{d\,{}^{D}W_L}{dx}\right)\frac{d\varphi_i^{(2)}}{dx}\frac{d\varphi_j^{(4)}}{dx}+\frac{1}{2}\left(\sum_{K=1}^{ND} {}^{D}\tilde{\tilde{B}}_{31}^{KJI}\frac{d\,{}^{D}W_K}{dx}\right)\varphi_i^{(2)}\frac{d\varphi_j^{(4)}}{dx}$$
$$+\left(\sum_{K=1}^{ND}\sum_{L=1}^{ND} {}^{D}\bar{\bar{D}}_{11}^{IKJL}\frac{d\,{}^{D}W_K}{dx}\frac{d\,{}^{D}W_L}{dx}\right)\frac{d\varphi_i^{(2)}}{dx}\frac{d\varphi_j^{(4)}}{dx}\Bigg]dx + K_{ij}^{(24)IJ}$$

$$T_{ij}^{(31)IJ} = K_{ij}^{(31)IJ}$$

$$T_{ij}^{(32)IJ} = \int_{x_a}^{x_b}\frac{1}{2}\left(\sum_{K=1}^{M} {}^{D}\hat{B}_{11}^{KJI}\frac{dW_K}{dx}\right)\frac{d\varphi_i^{(3)}}{dx}\frac{d\varphi_j^{(2)}}{dx}dx + K_{ij}^{(32)IJ}\ )$$

$$T_{ij}^{(33)IJ} = K_{ij}^{(33)IJ}$$

$$T_{ij}^{(34)IJ} = \int_{x_a}^{x_b}\left[\left(\sum_{K=1}^{M} {}^{D}\hat{\hat{B}}_{11}^{KJI}\frac{dW_K}{dx}\right)\frac{d\varphi_i^{(3)}}{dx}\frac{d\varphi_j^{(4)}}{dx}+\frac{1}{2}\left(\sum_{K=1}^{ND} {}^{D}\bar{\bar{B}}_{11}^{IKJ}\frac{d\,{}^{D}W_K}{dx}\right)\frac{d\varphi_i^{(3)}}{dx}\frac{d\varphi_j^{(4)}}{dx}\right]dx$$
$$+K_{ij}^{(34)IJ}$$

$$T_{ij}^{(41)IJ} = \int_{x_a}^{x_b}\left(\sum_{K=1}^{M} {}^{D}B_{11}^{JKI}\frac{dW_K}{dx}\right)\frac{d\varphi_i^{(4)}}{dx}\frac{d\varphi_j^{(1)}}{dx}dx + K_{ij}^{(41)IJ}$$

$$T_{ij}^{(42)IJ} = \int_{x_a}^{x_b}\Bigg[\left(\sum_{K=1}^{M}\sum_{L=1}^{M} {}^{D}D_{11}^{JKLI}\frac{dW_K}{dx}\frac{dW_L}{dx}\right)\frac{d\varphi_i^{(4)}}{dx}\frac{d\varphi_j^{(2)}}{dx}+\left(\sum_{K=1}^{M} {}^{D}\tilde{B}_{13}^{KIJ}\frac{dW_K}{dx}\right)\frac{d\varphi_i^{(4)}}{dx}\varphi_j^{(2)}$$
$$+\frac{5}{2}\left(\sum_{K=1}^{M}\sum_{L=1}^{ND} {}^{D}\bar{D}_{11}^{JKIL}\frac{dW_K}{dx}\frac{d\,{}^{D}W_L}{dx}\right)\frac{d\varphi_i^{(4)}}{dx}\frac{d\varphi_j^{(2)}}{dx}$$
$$+\frac{1}{2}\left(\sum_{K=1}^{ND}\sum_{L=1}^{ND} {}^{D}\bar{\bar{D}}_{11}^{JIKL}\frac{d\,{}^{D}W_K}{dx}\frac{d\,{}^{D}W_L}{dx}\right)\frac{d\varphi_i^{(4)}}{dx}\frac{d\varphi_j^{(2)}}{dx}\Bigg]dx + K_{ij}^{(42)IJ}$$

$$T_{ij}^{(43)IJ} = \int_{x_a}^{x_b}\left(\sum_{K=1}^{M} {}^{D}\hat{\hat{B}}_{11}^{KIJ}\frac{dW_K}{dx}\right)\frac{d\varphi_i^{(4)}}{dx}\frac{d\varphi_j^{(3)}}{dx}dx + K_{ij}^{(43)IJ}$$

$$T_{ij}^{(44)IJ} = \int_{x_a}^{x_b} \left[\left(\sum_{K=1}^{N} {}^{D}\bar{B}_{11}^{KIJ} \frac{dU_K}{dx} \right) \frac{d\varphi_i^{(4)}}{dx} \frac{d\varphi_j^{(4)}}{dx} + \frac{1}{2} \left(\sum_{K=1}^{M} \sum_{L=1}^{M} {}^{D}\bar{D}_{11}^{LKIJ} \frac{dW_K}{dx} \frac{dW_L}{dx} \right) \frac{d\varphi_i^{(4)}}{dx} \frac{d\varphi_j^{(4)}}{dx} \right.$$
$$+2 \left(\sum_{K=1}^{M} \sum_{L=1}^{ND} {}^{D}\bar{\bar{D}}_{11}^{KIJL} \frac{dW_K}{dx} \frac{d\,{}^{D}W_L}{dx} \right) \frac{d\varphi_i^{(4)}}{dx} \frac{d\varphi_j^{(4)}}{dx} + \left(\sum_{K=1}^{M} {}^{D}\tilde{\tilde{B}}_{13}^{IJK} W_K \right) \frac{d\varphi_i^{(4)}}{dx} \frac{d\varphi_j^{(4)}}{dx}$$
$$+ \left(\sum_{K=1}^{ND} {}^{D}\bar{\bar{B}}_{11}^{IKJ} \frac{d\,{}^{D}U_K}{dx} \right) \frac{d\varphi_i^{(4)}}{dx} \frac{d\varphi_j^{(4)}}{dx} + \frac{1}{2} \left(\sum_{K=1}^{M} \sum_{L=1}^{ND} {}^{D}\bar{\bar{D}}_{11}^{KILJ} \frac{dW_K}{dx} \frac{d\,{}^{D}W_L}{dx} \right) \frac{d\varphi_i^{(4)}}{dx} \frac{d\varphi_j^{(4)}}{dx}$$
$$\left. + \left(\sum_{K=1}^{ND} \sum_{L=1}^{ND} {}^{D}\bar{\bar{D}}_{11}^{IJKL} \frac{d\,{}^{D}W_K}{dx} \frac{d\,{}^{D}W_L}{dx} \right) \frac{d\varphi_i^{(4)}}{dx} \frac{d\varphi_j^{(4)}}{dx} \right] dx + K_{ij}^{(44)IJ} \qquad (16)$$

The tangent stiffness matrix is symmetric.

3. VERIFICATION OF THE FINITE ELEMENT MODEL

3.1 Stress Analysis

A laminated beam of $[90_m / 0_n / 90_m / 0_n]_s$ lay-ups with pre-delamination through the width in the mid-plane is considered as an example to demonstrate the accuracy of solutions using the layerwise theory taking into account delamination (LWTDEL). The laminated beam is subjected to three-point-bending and the problem definitions are taken from Zhao *et al*.[21]. The configurations and the boundary conditions of the problem are displayed in Figure 2. The delaminated interface is assumed to preexist in the mid-plane and the interfacial crack length, *a*, is set to 10mm. The total length of the beam, *L*, is 90mm, and the total thickness of the laminate, *h*, is 4mm. Noting the beam is symmetric about the beam center, half of the beam shown in Figure 2 is modeled. The material properties of NCT-301 graphite/epoxy composite used in this numerical example are same as in [21], which are

$$E_1 = 145\,\text{GPa} \qquad E_2 = E_3 = 10.7\,\text{GPa}$$
$$G_{12} = G_{13} = 4.5\,\text{GPa} \qquad G_{23} = 3.6\,\text{GPa}$$
$$\nu_{12} = \nu_{13} = 0.3 \qquad \nu_{23} = 0.49$$

The interlaminar shear stress distributions near the delaminated mid-plane along the beam length for the case of $m = n = 4$ and the static bending load q_0 applied at the beam center are presented in Figure 3. The stress values are normalized by $\tau_0 = 3q_0 / 4h$, where h is the total thickness (4mm) of the laminated beam.

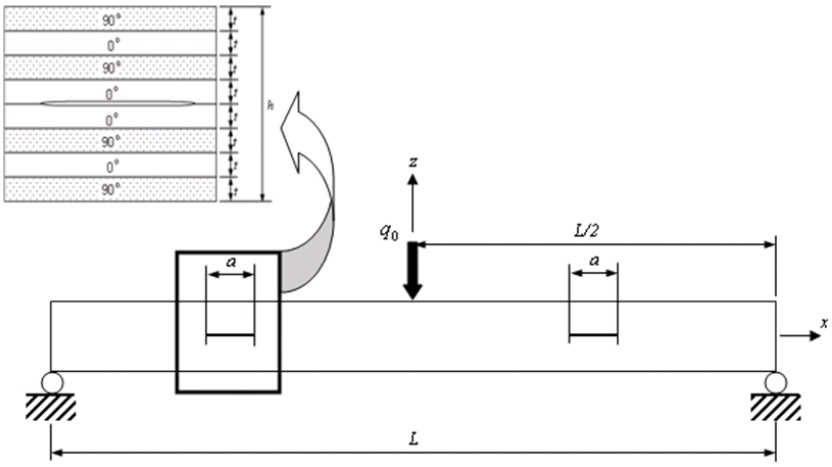

Figure 2. Configurations of laminated beam under three-point bending

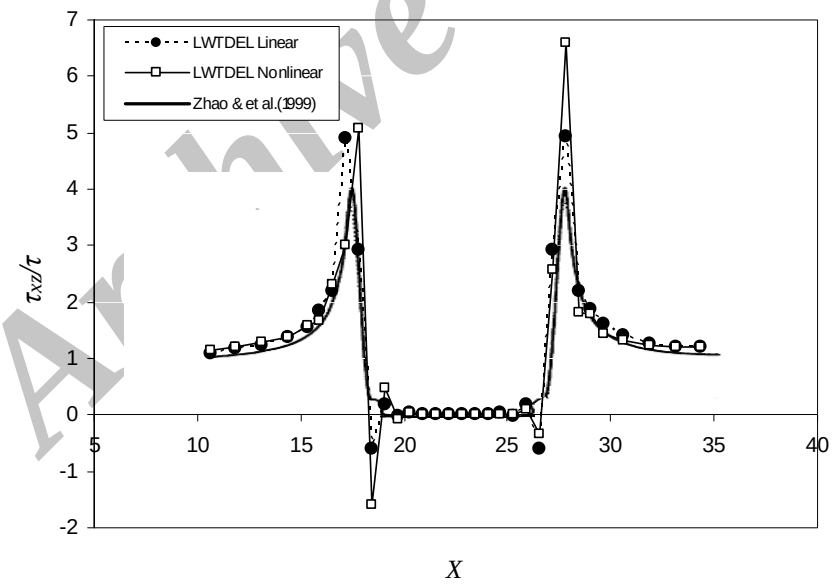

Figure 3. Nondimensional interlaminar shear stress $\overline{\tau}_{xz} = \tau_{xz} / \tau_0 = (4h\tau_{xz} / 3q_0)$ distribution near the delaminated mid-plane along the beam length (simply supported beam). [$\overline{\tau}_{xz}(x, -0.014088)$ when $q_0 = 400N / mm$]

In discretizing the domain, 36 linear beam elements are used along the beam length direction. Since each angle ply's thickness is uniform, 4 layers of each 0° ply and 90° ply are modeled as a single numerical layer using one quadratic interpolation function through the numerical layer's thickness. The selective reduced numerical integration scheme [20] is used for the transverse shear and transverse normal components of the coefficients in equations (14) and (16) to avoid shear locking. The solutions are obtained at the Gauss points nearest to the mid-plane of beam elements along the beam length.

As can be seen in Figure 3, a very good agreement is found between the solutions of LWTDEL and those of Zhao *et al.* [21]. The solution based on the linear strain fields and the solution of Zhao *et al* show a symmetric stress distribution about the interlaminar crack center, whereas the nonlinear solution of LWTDEL shows an unsymmetric stress distribution owing to the hardening effect caused by the nonlinearity.

3.2 Stress Intensity Factor

Once the delamination occurs in the composite beam, its growth is predicted by the fracture criterion such as the energy required to create the new surface. In the frame work of fracture mechanics, the strain energy release rate is often used to estimate the growth of the existing crack. The stress intensity factor, *K*, is invoked in his work for the plane stress case, and the relationship with the strain energy release rate, *G*, has been shown as

$$G = \frac{K^2}{E} \tag{17}$$

Poisson's ratio ν has to be taken into account for the case of plane strain [23]

$$G = \frac{K^2}{E}(1-\nu^2) \tag{18}$$

Fedderson [24] discussed analytical solutions for the finite width correction of the stress intensity factor($K/\sigma_0\sqrt{\pi a}$). He compared the various analytical solutions in tabular form and he concluded the solution of Isida [25] as the most precise expression.

In order to demonstrate the accuracy of computing the strain energy release rate using the layerwise theory, two numerical examples are considered here. The stress intensity factor is computed from equation (17), and the strain energy release rate *G* is obtained using the finite element model by following the virtual crack closure technique of Raju [26].

The cracked models are depicted in Figure 4. Plane stress boundary conditions are imposed on the single edge crack model and the center crack model. Since the examples are dealing with two dimensional plate models, the layerwise beam model developed in the previous chapter is attempted to compute the stress intensity factor. For the single edge crack model, the length of the crack *a* is varied in the computation from 0.2*b* to 1.0*b*, and for the center crack model, the crack *a* is varied from 0.1*b* to 0.5*b* while *b* and *L* are fixed to be same (*b*=*L*).

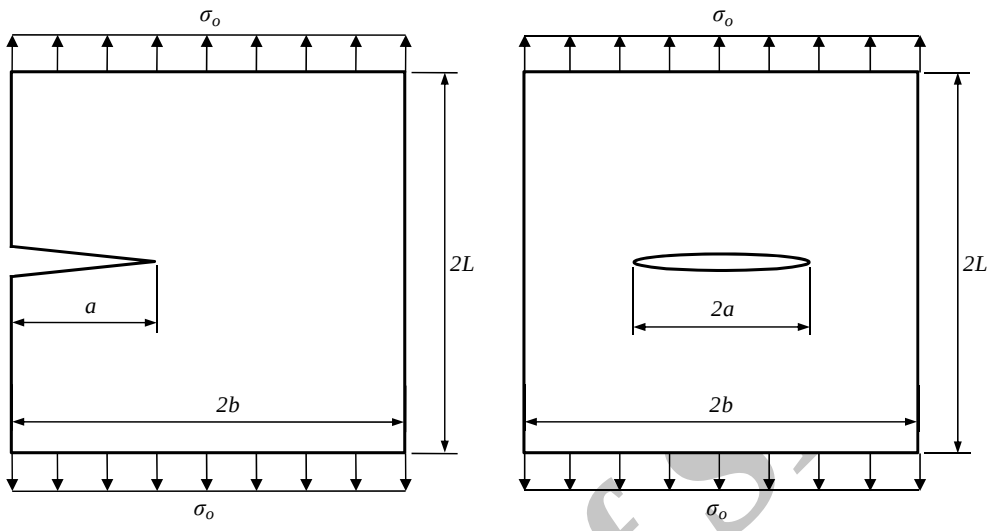

Figure 4. Single edge crack model (a) and center crack model (b)

As for the mesh using the layerwise beam finite element model, the thickness of the beam is considered as 2*L* and the length of the beam is treated as 2*b*. Since the material is homogeneous in the problem, material properties of each layer in the layerwise beam finite element model are treated as the same. The smallest elements are placed at the crack tip and the thickness of the layer which includes the crack face is set to be the smallest element length. The thickness of the layers and the size of the elements are varied in the computation in order to see how the numerical values are dependent on the mesh size. The quadratic shape functions are used for each beam element along the length (2*b*) and also the quadratic approximation functions are used for computing the coefficients through the thickness (2*L*) [14].

The results obtained from layerwise beam finite element model with other solutions available from the literature are presented in Table 1. The strain energy release rate has been converted to the stress intensity factor using equation (17), and again the stress intensity factor, *K*, is divided by a factor, $\sigma_0\sqrt{\pi a}$ [24].

Compared to the analytical solutions of Gross and Bowie[27], the stress intensity factors computed based on the virtual crack closure technique using the layerwise beam model shows less than 6% or 8% of discrepancy for all element sizes at the crack tip. Overall, the numerical values of the present model tend to overestimate slightly more when compared to the analytical values except for the case of $a/b = 0.2$. Further, the sensitivity of the stress intensity factor to the finite element size does not appear significant.

The numerical values show a good agreement with the analytical values within 5% of error even with the same length for all elements including the crack tip region. However the relationship between the crack tip element length (Δ) with the crack length ratio to the total

length of the model (*a/b*) is worth studying in order to find a criterion for constructing the meshes. When the ratio of $\Delta/(a/b)$ is around 0.1, the computed values show a good agreement with the results from the literature. Hence, the effort to build extremely fine meshes does not seem to be required to obtain acceptable values of the strain energy release rate or the stress intensity factor.

Table 1. Finite width corrections of stress intensity factor $\frac{K}{\sigma_0\sqrt{\pi a}}$ for a single edge crack

a/b	Virtual Crack Closure Using Layerwise Beam FEM					Gross	Bowie
	Δ=0.1b	Δ=0.05b	Δ=0.02b	Δ=0.01b	Δ=0.001b		
0.2	1.14	1.16	1.17	1.17	1.17	1.19	1.20
0.4	1.39	1.40	1.41	1.41	1.42	1.37	1.37
0.6	1.73	1.75	1.76	1.76	1.76	1.66	1.68
0.8	2.18	2.20	2.21	2.21	2.21	2.12	2.14
1.0	2.82	2.84	2.86	2.86	2.86	2.82	2.86

Comparison between the stress intensity factors computed from layerwise beam finite element model with the ones available from the literature is presented in Table 2.

Table 2. Finite width corrections of stress intensity factor $\frac{K}{\sigma_0\sqrt{\pi a}}$ for a center crack

a/b	Virtual Crack Closure Using Layerwise Beam FEM					Hellen	Isida
	Δ=0.1b	Δ=0.05b	Δ=0.02b	Δ=0.01b	Δ=0.001b		
0.1	0.90	0.95	0.96	0.96	0.97	1.02	1.00
0.2	0.98	1.00	1.00	1.00	1.01	1.05	1.03
0.3	1.05	1.06	1.07	1.07	1.07	1.15	1.06
0.4	1.14	1.15	1.16	1.16	1.16	1.21	1.13
0.5	1.25	1.27	1.27	1.27	1.27	1.33	1.27

Analytical solutions for an infinitely long strip with center crack are found in many works and the solution of Isida was tabulated as a representative analytical solution. As for a finite *L*, Hellen [28] obtained the numerical solutions for the case of $b = L$ based on the virtual crack extension method, and his solutions are compared in Table 2. The present analysis shows underestimated values relative to the solutions of Hellen by about 4 to 8% except for *a/b*=0.2. Considering that the numerical solutions in the literature calculated with a different ratio of *L/b* and they are often compared to the analytical solutions which are based on the case of $L \to \infty$, the discrepancy of the present analysis appears to be accurate

enough to be used for computing the strain energy release rate or the stress intensity factors. In addition, underestimation of the stress intensity factor using the virtual crack closure technique has been also observed by Raju in his study and his optimized meshes shows about 4% discrepancy [26]. The size of the crack tip elements, again, does not appear to affect the numerical values drastically when the crack tip element size is relatively small enough. In the present study, the optimal size of the crack tip element appears to be 0.1a and the smaller element size makes little change in accuracy of the stress intensity factors.

4. DELAMINATION AND BOUNDARY CONDITIONS

The combination of load type and boundary condition appears to affect the response of delamination analysis under bending loads. Four types of bending tests are considered to evaluate the influence of boundary conditions on the delamination behavior in composite laminated beams. The beams are composed of $[90_m/0_n]_S$ cross ply laminates and an interlaminar crack with the length of a is assumed to exist at the tip of pre-existing transverse crack (see Figure 5).

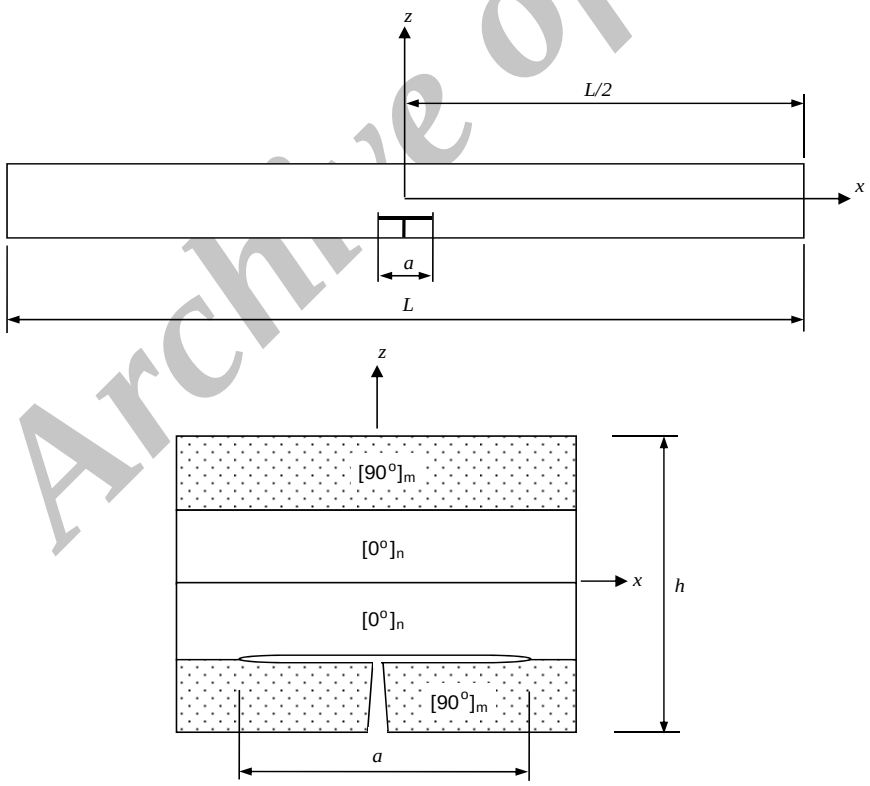

Figure 5. Laminated beam with a delamination originated from a transverse crack

The single transverse crack is assumed to be aligned with the *z*-axis in the 90-degree layers on the tensile side of the beam and it is also assumed to run through the width of the beam completely. As shown in Figure 5, an interlaminar crack at the interface of the cracked 90-degree layer and the adjacent 0-degree layer is assumed to be located symmetrically about the *z*-axis. One can expect to simulate a crack similar to the delamination originated from a free edge of the beam under bending.

The material properties of the composite are taken from [29] and they are as follows:

$$E_1 = 156\,\text{GPa} \qquad E_2 = E_3 = 9.09\,\text{GPa}$$
$$G_{12} = G_{13} = 6.96\,\text{GPa} \qquad G_{23} = 3.24\,\text{GPa}$$
$$\nu_{12} = \nu_{13} = 0.228 \qquad \nu_{23} = 0.4$$

The numerical computation to obtain the strain energy release rate for each boundary condition is performed using the LWTDEL code, which has been developed based on the layerwise beam theory including delamination. In the numerical model, half of the beam is modeled using the geometric symmetry and the assumption of symmetric crack growth.

Four different boundary conditions are considered to impose bending loads on the specimen: a) 3-point bending, b) clamped-ends with center load, c) distributed load with simply supported ends and d) 4-point bending (see Figure 6). The applied load in each case is such that the maximum bending moment produced in the beam is the same for all four boundary conditions. For lay-ups of $[90_2 / 0_2]_S$, the thickness of each ply is assumed to be 0.5mm, total thickness of the beam as 4mm, and the length of the beam as 150mm. The moment arm, *S*, for the case of 4-point bending is taken as 5mm.

4.1 Role of Bending Moment

Figure 7 presents the strain energy release rate versus the delamination length for each boundary condition. Unlike the axial extension test in which the strain energy release rate usually increases and approaches an asymptotic value as the delamination length increases [8, 11, 15], the strain energy release rate shows different patterns in the bending test according to the type of boundary condition.

For the case of distributed load with simply supported ends and 3-point bending, the strain energy release rate keeps decreasing as the delamination length grows. For the case of clamped ends, the strain energy decreases until the delamination length reaches a little less than half of the beam length, then it starts increases again. Only for the case of 4-point bending, the strain energy remains almost constant except for the very short delamination length. Based on this observation, the length of the delamination crack does not seem to directly contribute to the variation of strain energy release rate. Rather, the strain energy release rate is governed by the location of the delamination crack tip at which the amount of bending moment is determined by the boundary condition.

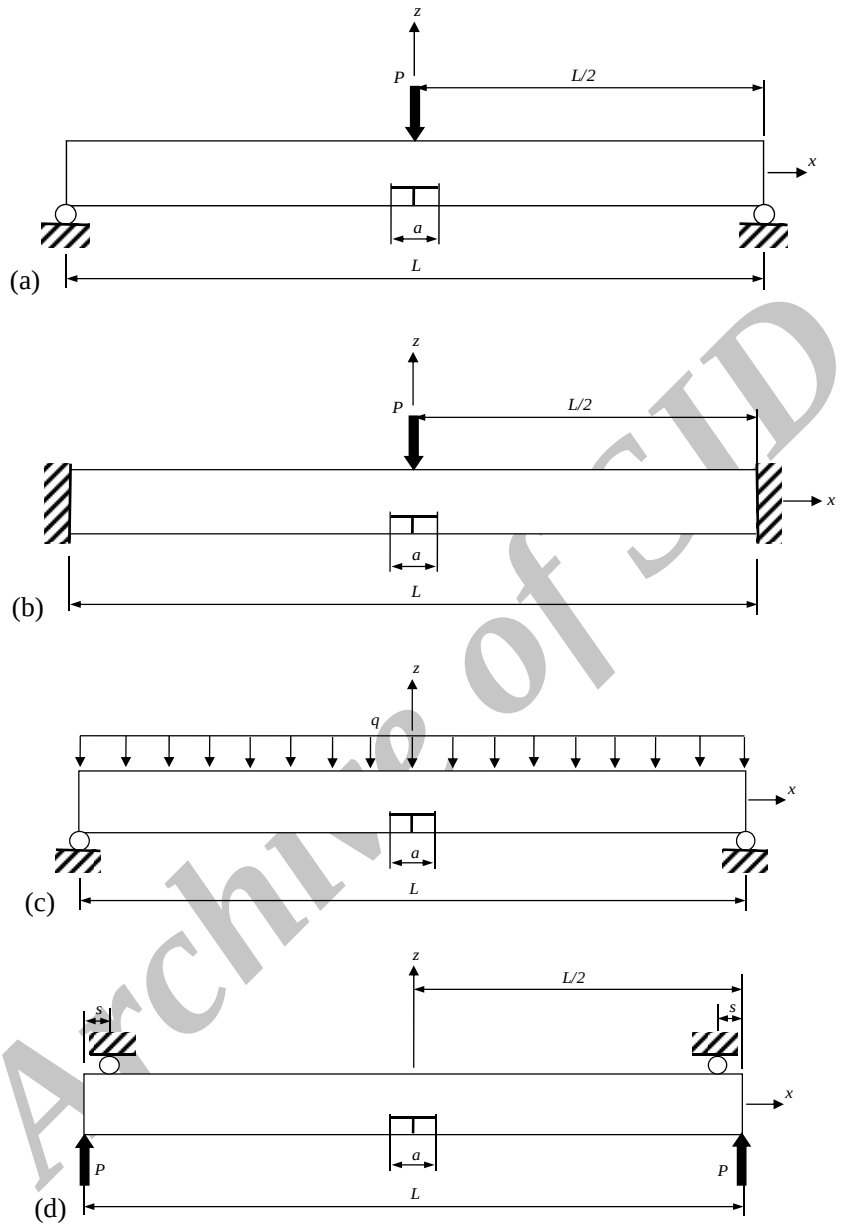

Figure 6. Four boundary conditions (a) 3-point bending (b) clamped-ends with center load (c) distributed load with simply supported ends (d) 4-point bending

It is clear from Figure 7 that the strain energy curve pattern resembles the bending moment along the beam (see Figure 8). As the crack tip moves from the beam center toward the beam ends, the bending moment at the position of the crack tip varies and the strain energy release rate varies proportionally to the bending moment. In particular, the bending moment for the case of four-point bending is uniform in between the inner supports, which gives the uniform strain energy release rate throughout the range of delamination length. In that perspective, the four-point bending test can be seen as a method to provide the boundary condition in which the delamination under bending can be analyzed without the boundary effect. Another interesting observation from Figure 7 is that the maximum value of the strain energy release rate obtained for the clamped ends is significantly larger than those of other three boundary conditions even though the vertical loads are applied so that the maximum bending moment can be the same for all four boundary conditions.

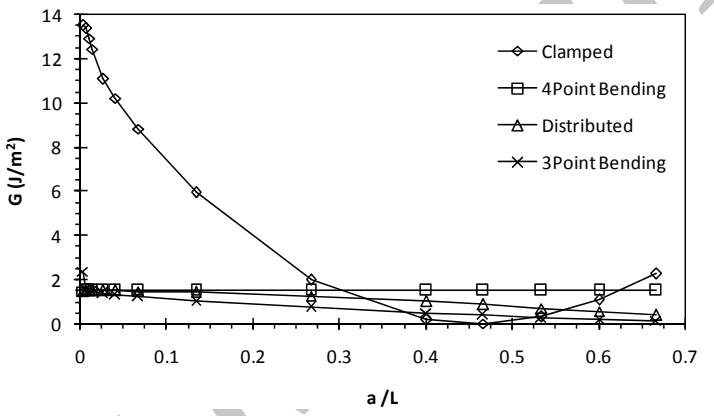

Figure 7. Strain energy release rate versus nondimensional delamination length

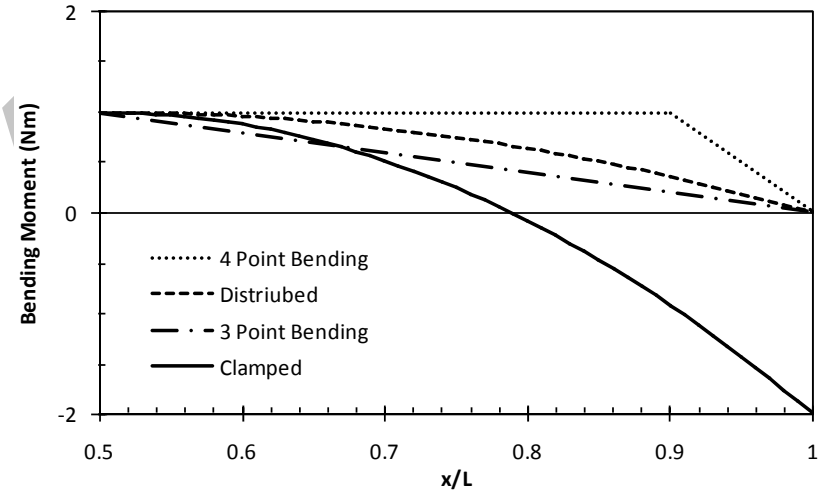

Figure 8. Bending moement distribution along the beam

4.2 Fracture Modes

Mixture of fracture Mode I and II in delamination have been observed and analyzed in the literature [11, 13, 17]. In order to make a distinction between the two modes, the strain energy components G_I and G_{II} are computed separately at a crack tip and then the total strain energy release rate G is obtained by the algebraic summation of G_I and G_{II}

$$G = G_I + G_{II} \tag{19}$$

Depending on the configuration of the laminate lay-ups or the loading conditions, a predominant mode is considered as the main mechanism to drive the delamination in the situation. More often than not, the total strain energy release rate is replaced by the predominant mode's strain energy release rate [10, 17, 30]. This simplification can be made to save the computational effort when the contribution of the other mode is negligibly small. To investigate the possibility of applying this simplification to the bending case, the following results are discussed.

For the four boundary conditions given in Figure 6, the fraction of the fracture modes to the total strain energy release rate is quantified in Figure 9. As seen in Figure 9, the fracture Mode I appears to be the main mechanism of the delamination for the given situation. Except for the case of clamped ends, G_I commonly takes up about 78% of the total strain energy release rate regardless of the delamination length. The remaining 22% of the total strain energy release rate can be seen as a contribution of the fracture Mode II. In this case, whether G_{II} is negligible is questionable. The error of 22% in evaluating the total strain energy release rate to predict the growth of delamination can result in a considerable underestimation. Thus, the mixture of Mode I and II should be taken into account to compute the total strain energy release rate, G, at the delamination crack tip under the given bending loads. A similar observation has been made by Murri and Guynn [30]. In their work, they tried to find the critical strain energy release rate at which the growth of delamination occurs, under different bending test conditions. However, they failed to connect the strain energy release rate to the bending moment. More importantly, the contribution of Mode II to the total strain energy release rate was underestimated and they argued that the critical strain energy release rate could be regarded as the value of Mode I.

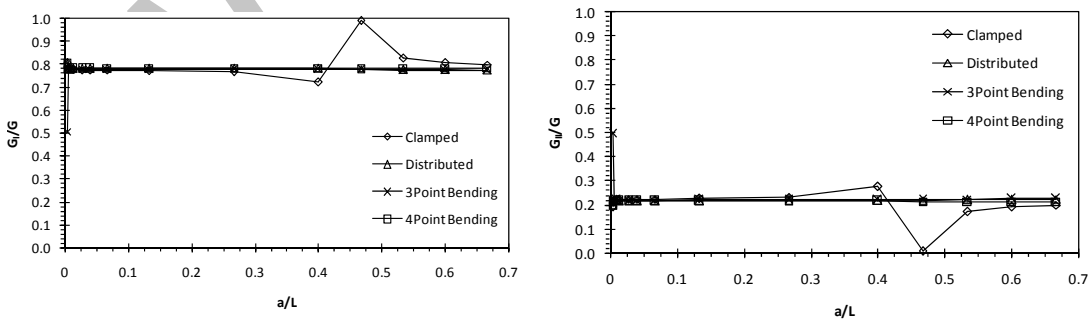

(a) (b)

Figure 9. Strain energy release rate fraction of (a) Mode I (b) Mode II

5. DELAMINATION UNDER PURE BENDING

In most of the studies related to the delamination damage, geometric nonlinearity in the specimen is neglected. The effect of the von Kármán type nonlinear strain field will be examined in this section by comparing the analysis based on the conventional linear strain fields. Since the computer code LWTDEL has been developed in a way that the nonlinear strain fields can be included in the delamination analysis, the influence of the geometric nonlinearity on the interlaminar cracks will be considered. In this study, the linear analysis refers to the numerical analysis based on the linear strain fields and the nonlinear analysis refers to the one based on the von Kármán type nonlinear strain fields. Also, as seen in the previous section, the four-point bending appears to be the boundary condition that can simulate the behavior of delaminated beam under the pure bending load. Based on these ideas, the lay-ups of $[90_2/0_2]_S$ are employed to model the laminated beams and the pre-existing interlaminar crack with length a is assumed at the interface of 90-degree and 0-degree on the tension side.

5.1 Delamination Growth

The change of strain energy release rate is presented in Figure 10 as the delamination length increases. The solid lines indicate the values computed from linear analysis and the dotted lines indicate the results from nonlinear analysis. As seen in the figure, the difference between the linear and nonlinear solution is negligible. Taking into account the von Kármán type nonlinearity in the delamination growth has little influence on the strain energy release rate G for the examples presented herein.

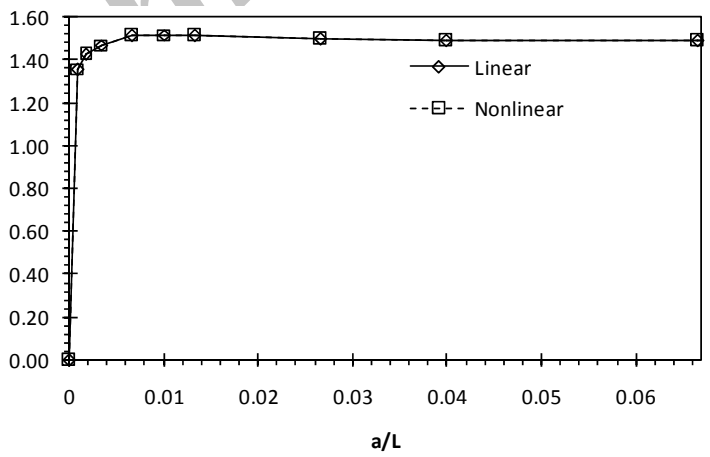

Figure 10. Strain energy release rate VS delamination growth under pure bending

When the delamination length a is less than $0.05L$, the strain energy release rate sharply decreases until it reaches a certain bounded value. The interlaminar crack length 0.05L is also approximately same as twice the thickness of one ply. Wang et al.[11] introduced the concept of effective flaw for analysis of the delamination onset in the axial tensile test and they made use of the asymptotic value that the strain energy release rate reaches, to determine the minimum size of the embedded delamination crack as the effective flaw in the analysis. Wang *et al.* [11] suggested twice the ply thickness as the size of effective flaw. The size of crack at which the strain energy release rate reaches a certain asymptotic value coincides with the present result under the bending load.

The primary fracture mode leading the delamination growth can be found in Figure 11 displaying the strain energy release rate fraction of Mode I and Mode II. Mode I has been identified as the primary fracture mode responsible for the delamination with transverse crack in 90-degree layer in the previous section. The strain energy release rate fractions remain constant even the interlaminar crack runs more than half of the total beam length.

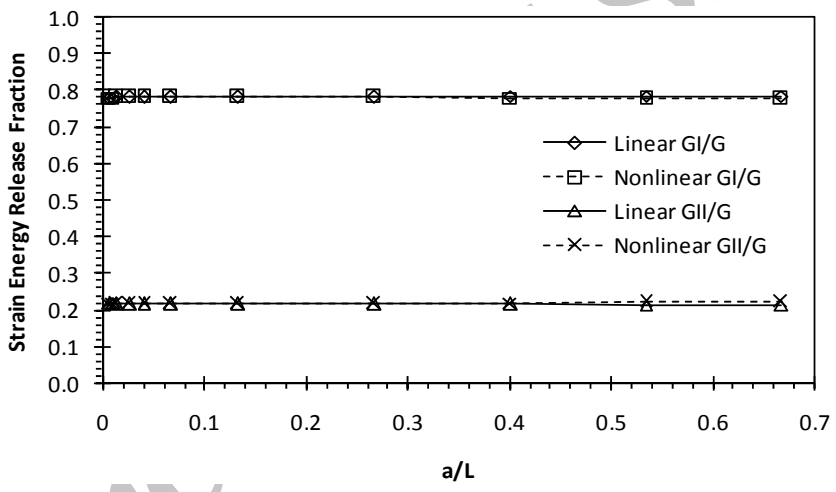

Figure 11. Strain energy release rate fraction VS delamination growth under pure bending

Next, influence of nonlinearity developed in the laminated beam, if any, under bending loads, is studied. The strain energy release rate ratios are defined as the ratios of the strain energy release rate from the linear analysis to the strain energy release rate from the nonlinear analysis. That is

$$R = \frac{G^N}{G^L}, \quad R_I = \frac{G_I^N}{G_I^L}, \quad R_{II} = \frac{G_{II}^N}{G_{II}^L} \tag{20}$$

where the superscripts L and N stand for the values from the linear and the nonlinear analysis, respectively.

The strain energy release rate ratios for the two cases of delamination are plotted as a function of delamination length in Figure 12. The strain energy release rate ratio of the

primary fracture mode, Mode I, decreases as the delamination length advances. On the other hand, the strain energy release rate ratio of the other fracture mode increases while the total strain energy release rate ratio is almost unchanged. This result implies that the nonlinearity is developed in the bending beam as the delamination crack grows, even if the change in the strain energy release rate due to nonlinearity is less than 5% for each fracture mode. However, the total strain energy release rate is found to be nearly unchanged during the delamination growth.

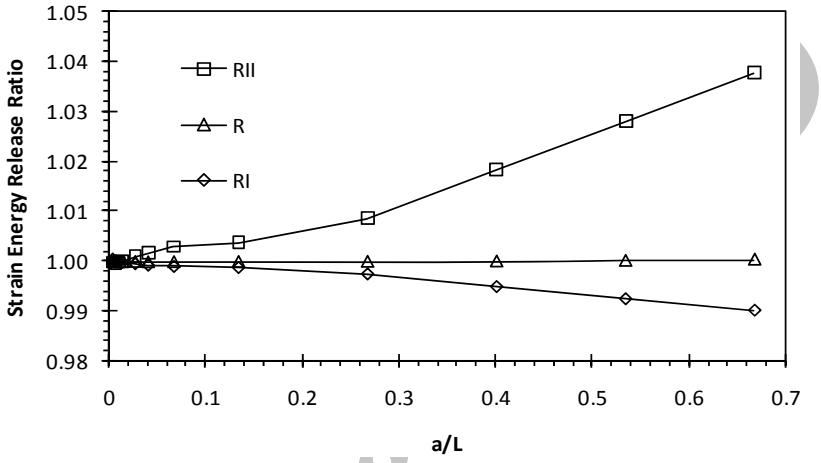

Figure 12. Strain energy release rate ratio VS delamination growth under pure bending

5.2 Applied Bending Moment

Figure 13 presents the relationship between the strain energy release rate and the applied bending moment when the interlaminar crack length is fixed. Again, the difference between the linear and nonlinear solutions appear negligible even when the strain energy release rate reaches a considerably high value. The strain energy release rate G is not much affected by including the nonlinearity throughout the whole range of the applied bending moment. This result can be related to the previous observation that the total strain energy release rate is little changed by the nonlinearity developed in the beam even though the strain energy release rate ratios of Mode I and Mode II are slightly changed. In that regard, the general perception that the delamination analysis is performed using the linear elasticity theory is justified.

Figure 14 shows information about the main fracture mode to drive the delamination as the applied bending moment is increased by displaying the strain energy release rate fractions of Mode I and Mode II. As seen previously, the primary fracture mode for the delamination is found to be Mode I throughout the range of applied bending moment for a fixed delamination length a =10mm. The contribution of the minor fracture mode to the whole delamination mechanism is not negligible. It deserves an attention that the strain energy release rate fraction is nearly constant for any value of applied bending moment if the delamination length is fixed.

The strain energy release rate ratio is plotted in Figure 15. Even though the change is small, it can be noticed that the strain energy release rate ratios increase as more bending moment is applied to the beam. This is due to the fact that the nodal force at the crack tip increases as the nonlinearity is introduced in the stiffness. It is worth remarking that the minor fracture mode, Mode II, shows more increase than the primary fracture mode, Mode I, as the applied moment increases.

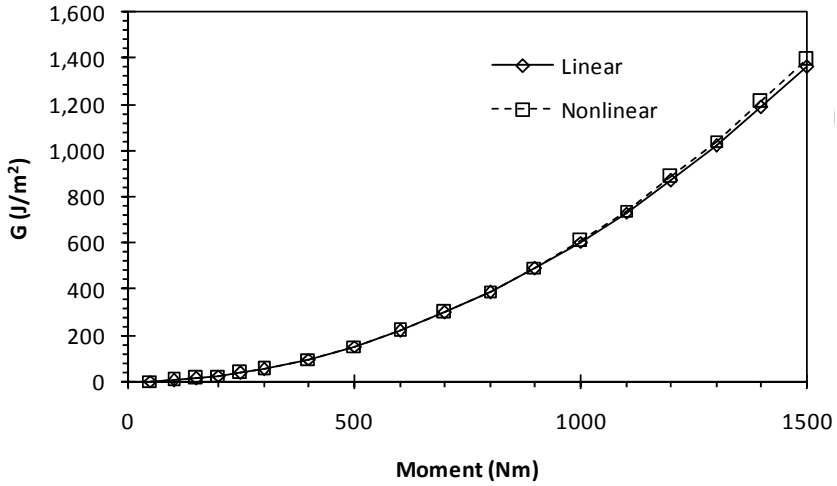

Figure 13. Strain energy release rate VS applied moment under pure bending (a=10mm)

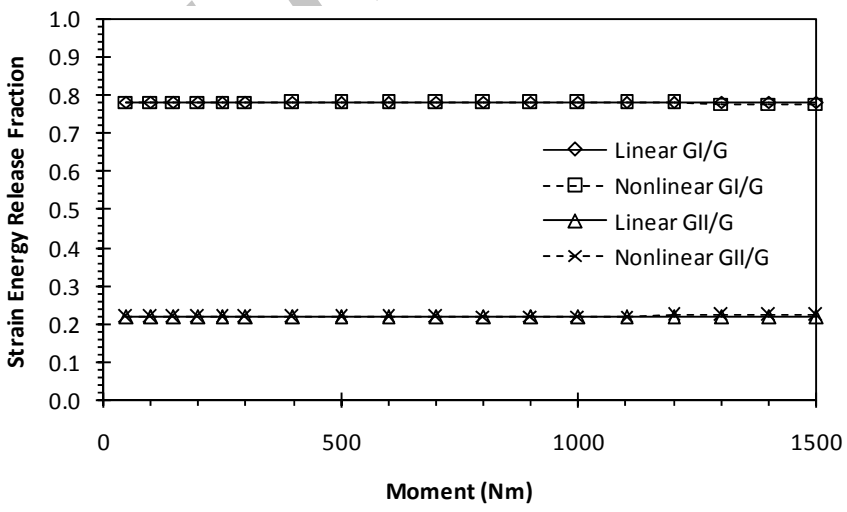

Figure 14. Strain energy release rate fraction VS applied moment crack under pure bending (a=10mm)

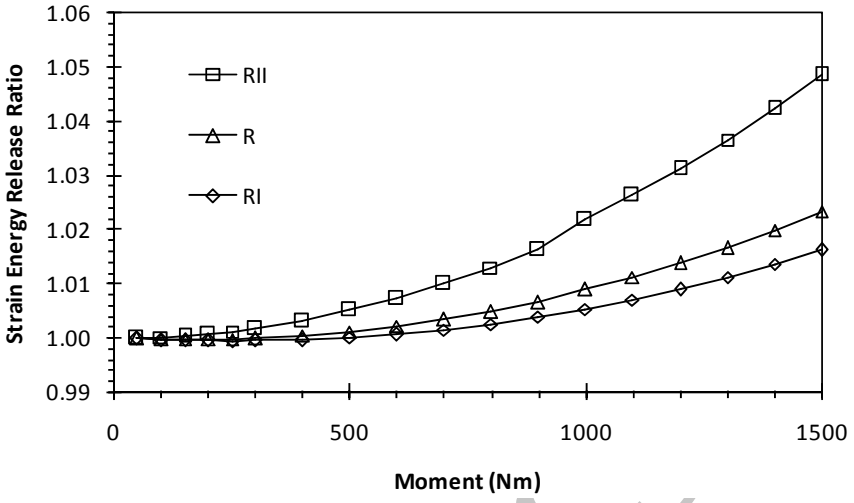

Figure 15. Strain energy release rate ratio VS applied moment under pure bending (a =10mm)

Overall, very little geometric nonlinearity in the beam is developed under the given bending load until the strain energy release rate reaches a very high value. The material used in this analysis is T300/976 graphite-epoxy composite and its critical strain energy release rate is reported in the range of $87.5\,J/m^2$ (for Mode I) to $282.6\,J/m^2$ (for Mode II) [31]. Although the strain energy release rate computed is well above these values, the nonlinear analysis shows almost the same G values as the linear analysis. Therefore, the interlaminar crack under a pure bending load is expected to grow before the applied bending moment gets large enough for the significant geometric nonlinearity to be prominent.

6. CONCLUSIONS

The layer-wise beam model is extended to consider interlaminar discontinuity in the displacement through the thickness. The Heaviside step function is incorporated in the formulation of layer-wise beam model, which successfully evaluates the local stresses around the interfacial crack. This model enables the strain energy release rate to be computed with a good accuracy.

The virtual crack closure method in the frame work of fracture mechanics is regarded as a simple and accurate way to compute the strain energy release rate or the stress intensity factor of the cracked strip. In particular, the application to the beam finite element model based on the layer-wise theory has been attempted and the accuracy of the solutions is satisfactory within a certain percentage of error comparing to the analytical values. The size of the finite elements at the crack tip usually shows a low sensitivity to the stress intensity factor, but to achieve a better accuracy without losing the modeling efficiency for the various case studies, the ratio of the crack tip element to the crack length ratio should be

considered. In this study, only the homogeneous material has been examined for the sake of verifying the accuracy by comparing to the well known analytical results from the literature. However, the application of the virtual crack closure method combined with the layer-wise beam finite element model is capable of predicting the progress of delamination damage.

Two cases of delamination in $[90_m / 0_n]_S$ cross plies subjected to bending loads are investigated using the finite element method based on the layer-wise beam theory. The boundary conditions imposed on the beam to be subjected to the bending causes a significant effect on the delamination growth and the strain energy release rate strongly depends on the location of the delamination crack tip because the bending moment distribution along the beam is determined by the boundary condition. The effect of boundary condition can be avoided by applying four-point bending which simulates a pure bending condition.

An interlaminar crack originated from a transverse crack in the 90-degree ply on the tensile side is primarily led by the fracture Mode I and the strain energy release rate is nearly constant under pure a bending condition if the delamination length is larger than a critical size. However, the contribution of Mode II is not negligible, and, unlike the progression of delamination under a tensile load, mode mixture should be considered for analysis of delamination under a bending load.

Very little effects are induced to the behavior of the delaminated beam by taking into account the von Kármán type nonlinearity in the numerical analysis. In this regards, the growth of delamination can progress in a laminated beam under a bending load before nonlinearity due to a large rotational deformation is prominent. Thus, the general idea of linear analysis on delamination is numerically justified by comparing the results from linear and nonlinear analyses.

Acknowledgements: The research reported herein was carried out while the first author was supported by US Army Grant 45508-EG and Oscar S. Wyatt Endowed Chair.

REFERENCES

1. Pagano NJ, Pipes RB. Some observations on the interlaminar strength of composite laminates, *International Journal of Mechanics and Science*, **15**(1973)679-688.
2. Kim KS. Characteristics of Free Edge Delamination in Angle-Ply Laminate, *International Conference on Composite Materials* (ICCM-V), 1985, pp. 347-361.
3. Kim RY. Initiation of Free-Edge Delamination in Composite Laminates, *Mechanical and Corrosion Properties. A, Key Engineering Materials*, **37**(1989)103-136.
4. Brewer J, Lagace PA. Quadratic stress criterion for initiation of delamination, *Journal of Composite Materials*, **22**(1988)1141-1155.
5. Griffith, AA. Phenomena of rupture and flow in solids, *Royal Society of London: Philosophical Transactions*, **221**(1920)163-198.
6. Rice JE. Mathematical analysis in the mechanics of fracture, *Fracture - An Advanced Treatise*, Vol. 2, H. Liebowitz, ed., Academic Press, New York, 1968, pp. 191-311.
7. Gurtin ME. On the energy release rate in quasi-static elastic crack propagation, *Journal of Elasticity*, **9**(1979)187-195.

8. Wang ASD. Growth mechanisms of transverse cracks and ply delamination in composite lamintes, *Proceedings of ICCM-3*, 1980, pp. 170-185.
9. Crossman FW, Wang ASD. Dependence of transverse cracking and delamination on ply thickness in graphite/epoxy laminates, *Damage in Composite Materials*, ASTM Special Techanical Publication, **775**(1982)118-139.
10. Wang ASD, Kishore NN, Feng WW. On mixed mode fracture in off-axis unidirectional graphite-epoxy composites, *Progress in Science and Engineering of Composites*, ICCM-IV, 1982, pp. 599-606.
11. Wang ASD, Kishore, NN, Li CA. Crack development in graphite-epoxy cross-ply laminates under uniaxial tension., *Composites Science and Technology*, **24**(1985)1-31.
12. Johannesson T, Blikstad M. Fractography and fracture criteria of the delamination process, *Delamination and Debonding of Materials*, ASTM Sepcial Technical Publication, **876,** 1985, pp. 411-423.
13. O'Brien TK. Characterization of delamination onset and growth in a composite laminate, *Damage in Composite Materials*, ASTM Special Tech. Pub., **775**, 1982, p.67.
14. Hwu C, Kao CJ, Chang LE. Delamination fracture criteria for composite laminates, Critical strain energy release rate experimentally measured for CFRP specimen with pre-existing delamination cracks, *Journal of Composite Materials*, **29**(1995)1962-1988.
15. Sih GC, Paris PC, Irwin GR. On cracks in rectilinearly anisotropic bodies, *International Journal of Fracture Mechanics*, **1**(1965)189-203.
16. O'Brien TK. Mixed mode strain energy release rate effects on edge delamination of composites, *Effects of Defects in Composite Materials*, ASTM Special Technical Publication, **836**, 1984, pp. 125-142.
17. Wilkins DJ, Eisenmann JR, Camin RA, Margolis WS, Benson RA. Characterizing delamination growth in graphite-epoxy, *Damage in Composite Materials*, ASTM Special Techanical Publication, **775**, 1982, pp. 168-183.
18. Hahn HT. Mixed-mode fracture criterion for composite materials, *Composites Technology Review*, **5**(1983)26-29.
19. Reddy JN. *Mechanics of Laminated Composite Plates and Shells. Theory and Analysis*, 2nd ed., CRC Press, Boca Raton, FL, 2004.
20. Reddy JN. *An Introduction to Nonlinear Finite Element Analysis*, Oxford University Press, New York, 2004.
21. Zhao J, Hoa SV, Xiao XR, Hanna I. Global/Local Approach using Partial Hybrid Finite Element Analysis of Stress Fields in Laminated Composites with Mid-Plane Delamination Under Bending, *Journal of Reinforced Plastics and Composites*, **18**(1999)827-843.
22. Irwin GR. Analysis of stresses and strains near the end of a crack traversing a plate, *Journal of Applied Mechanics*, **24**(1957)361-364.
23. Broek D. *Elementary Engineering Fracture Mechanics*, Martinus Nijhoff publishers, Dordrecht, The Netherlands, 1986.
24. Fedderson C. Discussion on plane strain crack toughness testing, *Plane Strain Crack Toughness Testing of High Strength Metallic Materials*, ASTM Special Technical Publication, **410**(1967)77-79.

25. Isida M. On the tension of a strip with a central elliptical hole, *Transactions of the Japan Society of Mechanical Engineers*, **21**(1955)507-518.
26. Raju IS. Calculation of strain-energy release rates with higher order and singular finite elements, *Engineering Fracture Mechanics*, **28**(1987)251-274.
27. Bowie OL. Rectangular tensile sheet with symmetric edge cracks, *Journal of Applied Mechanics*, **31**(1964)208-212.
28. Hellen TK. On the method of virtual crack extension, *Internation Journal for Numerical Methods in Engineering*, **9**(1975)187-207.
29. Choi HY, Downs RJ, Chang FK. A new approach toward understanding damage mechanisms and mechanics of laminated composites due to low-velocity impact: Part I—Experiments, *Journal of Composite Materials*, **25**(1991)992–1011
30. Murri GB, Guynn EG. Analysis of delamination growth from matrix cracks in laminates subjected to bending loads, *Composite Materials: Testing and Design*, ASTM Special Technical Publication, **972**, 1988, pp. 322-339.
31. Liu S, Chang F. Matrix cracking effect on delamination growth in composite laminates induced by a spherical indenter, *Journal of Composite Materials*, **28**(1993)940-977.